X-612-67-524

NASA TM X-55995

MICRO-SCALE STRUCTURES IN THE INTERPLANETARY MEDIUM

LEONARD F. BURLAGA

SEPTEMBER 1967

NASA

GODDARD SPACE FLIGHT CENTER

GREENBELT, MARYLAND

MICRO-SCALE STRUCTURES IN THE INTERPLANETARY MEDIUM

Leonard F. Burlaga*

Laboratory for Space Sciences
NASA-Goddard Space Flight Center
Greenbelt, Maryland

September 1967

*NAS-NRC Postdoctoral Resident Research Associate

ABSTRACT

Micro-Scale Structures in the Interplanetary Medium

This report describes and analyses the following micro-scale ($\lesssim$ .01 AU) structures which were found in combined interplanetary magnetic field and plasma data obtained by the deep space probe, Pioneer 6: 1) Several types of simultaneous discontinuities in the magnetic field and plasma parameters; 2) at least one clear example of a transitional region (D-sheet) associated with a plasma discontinuity; 3) other D-sheets which give evidence of magnetic field annihilation; 4) inhomogeneous isothermal regions in which the square of the magnetic field intensity is proportional to the density; 5) periodic variations in the magnetic field intensity which are associated with discontinuities in the bulk speed. It is suggested that small velocity discontinuities play a fundamental role in reducing stresses in the interplanetary medium, and that large velocity discontinuities may give rise to waves and turbulence.

Micro-Scale Structures in the Interplanetary Medium

A. Introduction

Recently experimental results were published which suggest that several types of structures predicted by hydromagnetic theory (see Landau and Lifshitz, 1960) are present in the interplanetary medium. Indirect evidence for the existence of tangential discontinuities in the interplanetary medium, based on magnetic field data alone, was presented by Ness et al. (1966), Burlaga and Ness (1966) and by Siscoe et al. (1966). Indirect evidence for the existence of tangential discontinuities, based only on plasma data was given by Gosling et al. (1967). Mihalov et al. (1967) have shown that temperature peaks are sometimes associated with magnetic field discontinuities and have suggested that such heating may be produced by magnetic field annihilation.

This report presents simultaneous, high resolution plasma and magnetic field data, obtained by instruments on the deep space probe Pioneer 6, which demonstrate the existence of several distinct types of micro-scale ($\lesssim$ .01 AU) structures in the interplanetary medium. These structures will be discussed from the point of view of hydromagnetic theory and will be shown to satisfy certain necessary conditions for hydromagnetic structures.

B. Orbit and Instruments

The Pioneer 6 spacecraft was launched toward the sun into heliocentric orbit on December 16, 1965. It penetrated to $\approx$ .81 AU in mid-May 1966, when it was 25° ahead of the earth relative to the sun, and later it moved away from the sun and still farther ahead of the earth. The interplanetary medium was monitored essentially continuously from the date of launch through April 1966. Thereafter, data were transmitted only intermittently.

The magnetometer which provided the magnetic field data that will be discussed below has been described by Ness, Scearce and Cantarano (1966). Briefly, it is a uniaxial fluxgate magnetometer, mounted at an angle of 54° 45' to the spacecraft spin axis which is nearly perpendicular to the ecliptic plane. The instrument zero-level was calibrated in flight by physically reversing the direction of the sensor by 180°. Each orthogonal component of the magnetic field vector is known to $\pm$ .24 gamma. A complete vector measurement, consisting of three axial measurements per spacecraft rotation, is transmitted on average every 1.5 sec. at the highest bit rate. The data were reduced to give $|\vec{B}| \equiv B$, θ and ϕ as a function of time, where these quantities were computed from thirty-second averages of the measured components. Here θ and ϕ give the direction of $\vec{B}$ in solar ecliptic coordinates, i.e., θ is the latitude angle measured with respect to the ecliptic plane (+ above the plane), and ϕ is the azimuth angle relative to the spacecraft sun line (ϕ = 0 when $\vec{B}$ is along the line and toward the sun, and increases as $\vec{B}$ moves toward the eastern hemisphere of the sun).

The plasma fluid parameters which are presented below were obtained by means of a probe that has been described by Lazarus, Bridge and Davis (1966). The detector is a Faraday cup with an energy-determining grid which gives fluxes in fourteen contiguous energy intervals. An ion flux spectrum was measured every thirty-two seconds, and transmitted at the rate of approximately one every seventy-one seconds, at the highest bit rate. The fluid parameters for the protons were obtained by fitting the measured spectra to a convected isotropic, Maxwell-Boltzman distribution. This reduction, which was carried out by the experimenters with the support of Dr. V. Formisano, will be described in a future publication of the MIT group. Until these details are available, the data are to be regarded as preliminary. For this reason the emphasis in this paper is on significant qualitative results. Values for the densities will be presented as integers, and are considered to be accurate to this approximation. Bulk speeds and thermal speeds will be quoted with preliminary estimates of their errors.

C. Equilibrium Regions

Theory.

By definition, the microstructure of the interplanetary medium is seen by viewing a three dimensional region of the medium on a scale of order .01 AU. The fluid state of such a region is specified at any instant by giving the magnetic field and the first three moments of the distribution functions for the protons, electrons and heavier particles at points throughout the region. If the curvature of the lines of force is small in a region, so that $(\vec{B}\cdot\nabla)\vec{B}$ can be neglected, then the motion perpendicular to the lines of force is governed by the equation

$$\rho \frac{dv_\perp}{dt} = -\nabla_\perp\left(p_\perp + \frac{B^2}{8\pi}\right) \tag{1}$$

where $\vec{v}$ is the velocity, p is the kinetic pressure, and B is the magnetic field intensity (see Parker, 1963, page 157).

If the distribution functions of the particles in a region are bi-maxwellian, then the region is in equilibrium in the sense that there is no acceleration perpendicular to $\vec{B}$ if and only if

$$\frac{B^2}{8\pi} + n_p kT_\perp + n_e kT_\perp' + n_\alpha kT_{\perp\alpha} = p = \text{constant}$$

where $T_\perp$, $T_\perp'$ and $T_{\perp\alpha}$ are the perpendicular temperatures of the protons, electrons and α particles, respectively, and n_p, n_e, and n_α are the corresponding densities. If α particles are neglected as a zeroth approximation and if charge neutrality is assumed so that $n_e = n_p \equiv n$, then

$$\frac{B^2}{8\pi} + nk\,(T_\perp + T_\perp') = p = \text{constant}.$$

For an isothermal, equilibrium region, this may be written in the form

$$B^2 = a - Sn \qquad (2)$$

where $a = 8\pi p$ and $S = 8\pi k\,(T_\perp + T_\perp')$. The last equation gives

$$\frac{T_\perp'}{T_\perp} = \left(\frac{S}{8\pi k}\,\frac{1}{T_\perp} - 1\right)$$

Hundhausen et al (1966) have found that the interplanetary medium is anisotropic with the temperature greatest in the direction of $\vec{B}$ and smallest perpendicular to $\vec{B}$; on the average they found $T_{max}/T_{av} \approx 1.4$. The data which will be used below does not give $T_\perp$, but rather the temperature T in the direction of the earth-sun line. In view of the result of Hundhausen et al., $T > T_\perp$. Thus, for an isothermal equilibrium region

$$\frac{T_\perp'}{T_\perp} \geq \left(\frac{S}{8\pi k}\,\frac{1}{T} - 1\right) \qquad (3)$$

where S is determined by (2). If α particles are not neglected, and if it is assumed that $n_\alpha = .04\, n_p$ and $T_{\perp\alpha} \approx 4T_{\perp p}$ (Hundhausen et al., 1966), then (3) is replaced by

$$\frac{T_\perp'}{T_\perp} \gtrsim \left(.93\,\frac{S}{8\pi k}\,\frac{1}{T} - 1.07\right). \qquad (4)$$

This obviously does not differ appreciably from (3) if $T_\perp'/T_\perp > > 1$.

Observations.

Since the interplanetary medium is convected nearly radially outward from the sun at a speed of approximately 400 km/sec, which is much greater than the spacecraft speed, a one-hour sample of the measured magnetic field describes a one dimensional "segment" of a region whose extent is of order .01 AU. Data for "thermal" electrons and heavy particles are not available so a segment can only be incompletely described at present. In this paper a segment will be specified as in Figure 1 by plotting $\vec{B}$ (magnetic field), n (proton density), v_T (proton thermal speed), and u (bulk speed) versus universal time for an interval on the order of one hour.

Figure 1 shows a segment of the interplanetary medium that passed the spacecraft between 0630 and 0730 on December 22, 1965. The segment is obviously inhomogeneous: B decreases from 8γ to 2γ while n increases from 12 cm^{-3} to 29 cm^{-3}. Figure 2 shows that B and n are anticorrelated such that (2) is satisfied. The segment is also isothermal in the sense that $v_T \approx$ constant. ($v_T \approx 20 \pm 2$ km/sec). Thus, Figure 1 shows a segment which satisfies two necessary conditions for a segment of an equilibrium region. If it is assumed that the electron temperature is also constant, then $T_\perp'$ can be calculated from (3) using S from Figure 2 and $T = mv_T^2/3k$ from Figure 1. With $S = (4.2 \pm .3) \times 10^{-10}$ (erg $^2/cm^3$) and $T = 1.6 \times 10^4$ °K it is found that $T_\perp'/T_\perp \gtrsim 6.4$ and $T' \approx 10^5$ °K. Thus it appears that in some regions the electrons may be considerably hotter than the protons. This is consistent with the theory of Sturrock and Hartle (1966).

Figure 3 shows a segment which is the complement of the one just described. This segment passed the spacecraft between 0350 and 0500 on December 22, 1965. It is isothermal with $v_T \approx 21 \pm 3$ km/sec; it is inhomogeneous, where now B tends to increase while n decreases; and again B^2 is proportional to n (see Figure 4). The slope of the line in Figure 4 is $S = (4.2 \pm .3) \times 10^{-10}$ (erg^2/cm^3) from which it is found that $T' \approx 10^5$ °K, $T_\perp'/T_\perp \gtrsim 6.5$, as before.

It was just shown that at times the electrons may be considerably hotter than the protons in the interplanetary medium. When $T_\perp' >> T_\perp$, the kinetic pressure is primarily due to the electrons, since $p_\perp = n_p kT_\perp + n_e kT_\perp'$ and $n_e = n_p$. Moreover, if $n_p kT_\perp = 0\ (B^2/8\pi)$, as is generally observed, it is evident that at times the electrons may produce the dominant term on the RHS of (1). Thus electrons may sometimes play a dominant role in the dynamics of the interplanetary medium.

D. Discontinuities

Theory.

The theory of discontinuities in an ideal magnetic fluid has been summarized by Landau and Lifshitz (1960), Colburn and Sonett (1966), and others. Among the predicted types of discontinuities are tangential discontinuities which have three characteristics: 1) there is no flux of matter through the surface of the discontinuity, 2) there is no component of $\vec{B}$ normal to the surface of the discontinuity, and 3) the total pressure is continuous across the discontinuity.

It is convenient to picture a tangential discontinuity in terms of two adjacent elemental, rectangular, flux tubes which lie parallel to the surface of the discontinuity. This is illustrated in Figure 5 for a special case when the flux tubes are mutually perpendicular. The density temperature and magnetic field intensity may differ in each of the elemental flux tubes subject to the constraint

$$\frac{B_1^2}{8\pi} + n_1 k(T_1+T_1') = \frac{B_2^2}{8\pi} + n_1 k(T_2+T_2'), \qquad (5)$$

where the subscripts 1 and 2 refer respectively to the flux tubes that arrive before and after the surface of the discontinuity, as shown in Figure 5. The ribbon of vectors in Figure 5 illustrates the fact that sometimes the field changes directions between the adjacent flux tubes by means of a rotation fan. Such rotation fans have been discussed by Siscoe et al. (1966) in the analysis of Mariner 4 magnetometer data. Rotation fans were found in a few of the discontinuities which will be considered below, but they will not be discussed further because they

occur on a scale on the order of one minute, which is below the resolution of the plasma data.

Several classes of tangential discontinuities can be distinguished on the basis of (5). Let the symbol (sign ΔB, sign Δn, sign ΔT) describe the qualitative changes in the magnetic field intensity, density, and proton temperature, respectively, across a discontinuity. Thus, the symbol (+--) denotes a discontinuity across which B increases ($B_2 > B_1$) while n and T decrease ($n_2 < n_1$, $T_2 < T_1$); the symbol (0,0,0) denotes a tangential discontinuity separating two identical, non-parallel flux tubes ($B_1 = B_2$, $n_1 = n_2$, $T_1 = T_2$, but $\vec{B}_1 / B_1 \neq \vec{B}_2 / B_2$); and so on. From consideration of the changes in B, n and T which are consistent with (5), one finds that three classes of tangential discontinuities can be distinguished: 1) Class TO, containing only (0 0 0); 2) class T2, containing (+ - 0) and all the permutations and reflections of this set (see Table 1); 3) class T3, containing (+ - +) and all of the permutations and reflections of this set, shown in Table 1. Additional classes are possible if one includes parameters for bulk velocity electrons, and other particles.

To identify a tangential discontinuity unequivocally, it must be shown that (5) is satisfied for the adjacent flux tubes. This is not possible at the present time because unambigious measurements of the electron temperature are not available. However, the existence of discontinuities with signatures which are given in Table 1 will be demonstrated below. Such a signature is a necessary but not a sufficient condition for the existence of a tangential discontinuity. On the other hand, if we assume that the hydromagnetic theory of discontinuities is applicable,

then all of the signatures in Table 1 except (0 0 0), (-+ +) and (+ - -) uniquely describe tangential discontinuities, i.e., a discontinuity with such a signature can only be a tangential discontinuity. The signature (0 0 0) may describe a tangential discontinuity or a rotational discontinuity. The signatures(- + +) and(+--) could describe tangential discontinuities, or a slow forward shock and a slow reverse shock, respectively.

According to the definition of a tangential discontinuity, the flux tubes in Figure 5 may move relative to one another along the surface of the discontinuity. Thus let us use the term "glide plane" to refer to an element of a surface of a tangential discontinuity. Relative motion of elemental flux tubes along a glide plane should be observed as a discontinuity in the bulk speed. To see this, refer to Figure 6 which shows a glide plane moving away from the sun with speed u^1, say. Let the velocities of the flux tubes relative to the glide plane be $\vec{v}_1$ and $\vec{v}_2$. The radial component of the plasma velocity on side 1 is $u^1 + v_1 \cos \alpha_1 \cos \bar{\phi} + v_1 \sin \alpha_1 \cos \bar{\theta} \sin \bar{\phi}$ and that on side 2 is $u^1 - v_2 \cos \alpha_2 \cos \bar{\phi} + v_2 \sin \alpha_2 \cos \bar{\theta} \sin \bar{\phi}$. The radial component of the plasma velocity is nearly equal to the bulk speed if $|\vec{v}_2 - \vec{v}_1|/u^1 << 1$. In this case, neglecting abberation, the difference in the bulk speed Δu across a glide plane is approximately

$$\Delta u = v_1 (\cos \alpha_1 \cos \bar{\phi} - \sin \alpha_1 \sin \bar{\phi} \cos \bar{\theta}) + v_2 (\cos \alpha_2 \cos \bar{\phi} - \sin \alpha_2 \sin \bar{\phi} \cos \bar{\theta}) \qquad (6)$$

This reduces to $\Delta u = 0$ if the plane of the discontinuity is perpendicular to the radial direction, i.e., $\theta = \phi = \pi/2$. If $v_1 = 0$, $\alpha_2 = \pi/2$,

$\bar{\phi} = \pi/2$, then $|\Delta u| = v_2 \cos \bar{\theta}$ In this case the component $v_2 \sin \bar{\theta}$ carries a plasma element above the ecliptic plane and thus away from the glide plane while the component $v_2 \cos \bar{\theta}$ carries it toward the discontinuity at such a rate that its distance from the discontinuity remains unchanged. It is evident from Figure 6 that the largest $|\Delta u|$ occurs when $\alpha_1 = \alpha_2 = \bar{\phi} = \bar{\theta} = 0$, in which case $|\Delta u| = v_1 + v_2$. Since Δu is just the radial component of the projection of the vector $\vec{v}_2 - \vec{v}_1$ on the ecliptic plane, it follows that

$$|\vec{v}_2 - \vec{v}_1| \geq |\Delta u| \qquad (7)$$

Observations of T2 Discontinuities.

Table 1 shows that there are six possible types of T2 discontinuities - three complementary pairs. Hydromagnetic theory predicts that tangential discontinuities and only tangential discontinuities can have such signatures. The following results demonstrate the existence of five types of T2 discontinuities in the interplanetary medium.

Each of the segments in Figure 1 and Figure 3 contains a remarkable "cascade" of T2 discontinuities. Moreover, these are complementary cascades in the sense that one consists of three (- + 0) discontinuities while the other consists of three (+ - 0) discontinuities. The interpretation that these are tangential discontinuities is supported by the results in the previous section which suggest that these discontinuities are embedded in isothermal, equilibrium regions. Note that the magnetic field direction does not change appreciably across the discontinuities, indicating that the adjacent flux tubes are nearly aligned even though their contents differ

greatly. The bulk speed u does not change appreciably across the (+ - 0) discontinuities, but it does increase together with the increase in density in two of the three (- + 0) discontinuities. The latter effect may be due to relative motions of the adjacent elemental flux tubes; it does not imply a flux of matter normal to the plane of the discontinuity.

Figure 7 shows a second set of T2 discontinuities, embedded in a segment of the interplanetary medium which passed the spacecraft between 0750 and 0850 on December 20, 1965. This set consists of a (- 0 +) discontinuity and its complement, a (+ 0 -) discontinuity. Note that the discontinuities combine in several ways with a third discontinuity at 0829 which cannot be classified because of the limited resolution of the plasma data. For example, the (- 0 +) discontinuity separates a region of high B and low T from a region with low B and high T. The (- 0 +) and (+ 0 -) discontinuities define a "filament" consisting of a rather complicated "flux tube" which is somewhat hotter and has a predominantly lower B than the surrounding flux tube. The (+ 0 -) discontinuity and the unidentified discontinuity at 0829 form the boundaries of a filament that is marked by its bulk speed, which is higher than in the surrounding regions, and by its magnetic field direction ϕ, which is 180° out of phase with the direction of the field in the sourrounding regions.

A third type of T2 discontinuity, a (0 + -) discontinuity, is shown on the right half of Figure 8. This passed the spacecraft at $\approx$ 0321 on January 28, 1966. It separates two rather uniform regions with different n, u, v_T, θ and ϕ, but with the same B. It can be visualized as two non-aligned flux tubes with the same B, but different n and T, which move relative to one another along the plane of discontinuity. No clear example of

the complementary discontinuity (0 - +) was found, but of course this does not mean that it does not exist.

T3 Discontinuities.

Table 1 shows that six types of T3 discontinuities are possible-again, three complementary pairs. The (- - +), (- + +) and the (+ - -) were not observed in the sample of $\approx$ 2000 hours of data which was examined. The existence of the remaining three types of T3 discontinuities is demonstrated below.

Figure 9 shows an outstanding T3 discontinuity which was detected at $\approx$ 0139 on March 28, 1966. The discontinuity has the signature (+ + -) which identifies it as a tangential discontinuity if we again assume that hydromagnetic theory applies. The contents in each of the adjacent flux tubes are markedly different in this case, but the tubes are nearly aligned.

A complementary pair of T3 discontinuities with the signatures (- + -) and (+ - +) is shown in Figure 10. These were observed at 1522 and 1536, respectively, on January 20, 1966. The absolute numerical values of the plasma data in Figure 10 are subject to rather large uncertainties, not indicated by the error bars, because the peak of the distribution function happened to fall nearly between two channels in the plasma probe. But the qualitative changes are real. Note that these discontinuities form the boundaries of a filament which contains a cool, dense plasma and which is embedded in a hot, low-density plasma. The density on either side of the filament is roughly the same; the magnetic field intensity behind the filament is higher than ahead, and the temperature shows the opposite behavior.

TO Discontinuities.

Only one type of TO discontinuity is possible viz, (000). From the point of view of hydromagnetics, such a signature could describe either a rotational discontinuity or a tangential discontinuity. If it is a tangential discontinuity, it consists of two elemental flux tubes which are identical but not parallel. A TO discontinuity is shown on the left in Figure 8.

In an earlier paper Burlaga and Ness (1966), who were working with magnetic field data alone, identified a class of discontinuities which they called directional discontinuities. Loosely speaking, this means a discontinuity in the magnetic field direction without regard to the magnitude of the magnetic field. Two directional discontinuities are shown in Figure 8. Figure 11, which is based on the data used by Burlaga and Ness, shows the distribution of the number of directional discontinuities as a function of the fractional change in B across a discontinuity. Clearly, B is nearly continuous across most directional discontinuities. An examination of the plasma data which were available for nearly half of these directional discontinuities showed no appreciable change in n, u, or v_T in most cases. Thus, most of these directional discontinuities have the signature (0 0 0). This leads to the important hypothesis that discontinuities in the magnetic field direction are usually not associated with discontinuities in the other fluid parameters, i.e., most interplanetary discontinuities are TO discontinuities.

Remarks

1. The results which were just presented were selected to give the clearest possible examples which demonstrate the existence of several types of discontinuities. No attempt was made in this study to determine

the distribution of these discontinuities. However, it seems worth noting that unlike D-sheets and waves which will be discussed below, discontinuities are frequently observed and are clearly fundamental to the structure of the interplanetary medium. Such discontinuities probably play an important role in the scattering of cosmic rays:

2. Figures in section D suggest the following hypotheses which are relevant to the study of the structure of the interplanetary medium:

a) Fluctuations of the magnetic field are greatest in regions where the magnetic field intensity is smallest; conversely, the unperturbed medium tends to be most uniform in regions where the magnetic tension is large. This hypothesis is suggested by Figures 1, 3, 7 and 10.

b) Glide planes play an important role in reducing stresses in the interplanetary medium by allowing disturbances to propagate as gliding flux tubes at speeds up to the Alfven speed. This is suggested by all of the segments in section D which show that the field is usually rather uniform near a discontinuity. The largest discontinuity in bulk speed observed in these discontinuities is $\Delta u = 40$ km/sec, shown in Figure 9. In every case the observed Δu is less than the Alfven speed.

E. D - Sheets

Theory.

Landau and Lifshitz (1960) show that in a medium with finite conductivity and finite viscosity, a sharp, tangential or rotational discontinuity should be replaced by a gradually widening transitional region in which the velocity and magnetic field change smoothly from one value to another. To illustrate the processes which may be involved in the formation of a transitional region, consider a tangential discontinuity formed by two antiparallel elemental flux tubes. Suppose that some physical process operates at the discontinuity which annihilates the antiparallel field lines. Then the field intensity will be zero or very small at the discontinuity, and the temperature will presumably tend to increase as the result of annihilation (i.e. conversion) of magnetic field energy. Additional magnetic field lines may drift toward the discontinuity carrying some matter with them. This matter will be deposited at the discontinuity and will contribute to the pressure in the transitional region. If the thermal conductivity is very high, the temperature increase in the transitional region may be small or negligible, but the density may be high. As the process continues the mass which is deposited would tend to be accumulated, unless it is ejected. Thus a jet of matter may be squeezed out by the incoming flux tubes.

If the flux tubes are not antiparallel, but are separated by an angle ω, an annihilation process would reduce the field intensity at the discontinuity to some value $B_{min} \neq 0$, where B_{min} depends on B_1, B_2 and ω. A simple vector diagram (see Figure 12) shows that if

$B_1 = B_2$, then

$$\frac{B_{min}}{B_1} = \cos \frac{\omega}{2} \tag{8}$$

Figure 12 shows that when $B_1 \neq B_2$

$$4 B_{min}^2 = B_1^2 + B_2^2 + 2 B_1 B_2 \cos \omega. \tag{9}$$

Burlaga and Ness (1966) found a number of structures, which they called D-sheets, that are characterized by a dip in B at a discontinuity in θ and ϕ, which satisfy (8). We shall now re-examine these D-sheets, using the plasma data which are now available.

Observations.

Figure 13 shows a D-sheet which is associated with a well-defined plasma discontinuity that was detected at $\approx$ 0819 on April 3, 1966. The signature of the discontinuity may be (+ - 0) or (+ - +), but in either case it is a tangential discontinuity according to MHD theory. There is a significant change in bulk speed across the discontinuity. There is also some evidence for heating and for a low bulk speed ($u \approx 388$ km/sec) at the discontinuity but this rests on only one point. The observed minimum field intensity in the D-sheet, $B_{min} = (1.3 \pm .3)\gamma$, agrees well with that calculated from the annihilation hypothesis, Equation (9), which gives $B_{min}=(1.5 \pm .5)\gamma$. Thus, Figure 13 apparently shows a transitional region associated with a tangential discontinuity, as described by Landau and Lifshitz (1960).

Figure 14 shows a remarkable D-sheet which passed the spacecraft near 0915 on January 21, 1966. This is distinguished by the large amount of magnetic field energy which vanishes at the directional

discontinuity, ($\approx 7 \times 10^{-10}$ ergs/cm^3). Unfortunately, the plasma data are rather sparce, and they are somewhat difficult to interpret because the bulk speed ($u \approx 515$ km/sec) happened to be very near the edges of adjacent energy channels of the plasma probe; this last fact may account for the peculiar point at 0851. The plasma data show that the temperature, density and bulk speed are highest where the magnetic field intensity is lowest. The minimum magnetic field intensity which was calculated from the annihilation hypothesis (Equation 8) using $B_1 = B_2 = (14.0 \pm .2)\gamma$ and $\omega = 166^\circ$ is $B_{min} = (1.7 \pm 2.0)\gamma$ which compares favorably with the measured $B_{min} = (3.5 \pm 1.0)\gamma$. These results are consistent with the model which was described above. It is interesting to note that again the field direction is rather uniform in this region, where the magnetic field pressure is dominant.

Burlaga and Ness (1966) showed six other D-sheets with various values of ω. Plasma data are available for four of these. The magnetic field data may be found in the paper just cited, and the plasma data are summarized in Table 2, which gives the averages u, n, and v_T for the points ten minutes before and ten minutes after the directional discontinuities as well as the values of u, n, and v_T at the discontinuities. There is no significant change in B, n or v_T across any of these D-sheets, but a significant change in u is found in two cases. On the other hand, the density is significantly enchanced at the discontinuity in every case except one, and that case is characterized by a small $\omega (\omega \approx 85^\circ)$ and a correspondingly small dip in B. No statistically significant enhancement in temperature is observed, but the errors are rather large and may mask a small temperature increase. Neither these data nor those which were presented in the earlier parts of this paper show strong temperature spikes associated with discontinuities, as Mihalov et al. (1967) have suggested.

F. Waves

Observations.

Figure 15 shows what appears to be a periodic wave in the interplanetary magnetic field intensity. It is eight cycles long and has an "apparent" period of 4.5 minutes. Since this wave is distorted by a gradually changing background field on which it is superimposed, the background field was calculated by taking running averages of B over the apparent wave period and was subtracted from the measured B to obtain the result shown in Figure 16.

Figure 16 clearly demonstrates the existence of a periodic wave in the interplanetary magnetic field intensity. The amplitude of the wave is rather small ($\approx .3\gamma$), but the individual points in Figure 16 should be accurate to $\lesssim .1\gamma$ if the field varies smoothly through the wave, because each of the points is computed from an average of twenty (20) vector measurements of $\vec{B}$. Note that the large minimum at 0526 coincides with a discontinuity in the magnetic field direction.

Periodic variations cannot be seen in the plasma data in Figure 15. The density appears to remain constant at $3/cm^3$, but recall that the nearest integral value for the density is used, so we can only say that the variation in density in the wave is less than approximately 20%. There is some indication that the temperature is highest near the minima of the wave, but the errors are large so the evidence is inconclusive. Likewise, no periodic change in the bulk speed is observed, but again the errors are large. In short, the plasma data presented here are not sufficiently refined to establish that the wave in Figure 15 is a hydromagnetic wave.

Note how the wave fits among the discontinuities which are shown in the segment in Figure 15. The discontinuity at 0513 has the signature (- + 0) which identifies it as a tangential discontinuity if hydromagnetic theory applies. The other discontinuities, which are marked by changes in the magnetic field direction, appear to have the signature (0 0 0). All three discontinuities seem to be associated with discontinuities in the bulk speed, but note the size of the error bars as indicated by the point at 0507.

Another intersting compressional wave nested among three discontinuities is shown in Figure 17. Again the apparent period is on the order of five minutes (actually three minutes in this case), but now it seems to consist of two parts. Part I shows only a small variation in B and no fluctuation in ϕ and θ; it is nested in a filament between 0125 and 0140, and follows a large bulk speed discontinuity. Part II is nested in an adjacent filament and is characterized by large amplitude periodic changes in both the magnitude and direction of $\vec{B}$. Figure 18, which gives the θ, ϕ coordinates of successive thirty-second averages of magnetic field vectors from 0142.5 (point 1) to 0151 (point 17), shows that part II of the wave is polarized, i.e., the magnetic field vector rotates about the mean direction of $\vec{B}$ with the same frequency as the compressional oscillation. Figure 17 shows that there are statistically significant peaks in the bulk speed at minima in B.

Figure 19 shows a segment of the interplanetary medium that passed the spacecraft between 0300 and 0350 on December 22, 1965. A D-sheet with its associated directional discontinuity and a discontinuity in the bulk speed are imbedded in the center of the segment and are followed by a damped wave in the magnetic field intensity. The observed jump in bulk speed is rather small ($\approx$ 10 km/sec), but the glide plane (assuming that we are dealing with a tangential discontinuity) is nearly normal to

the bulk velocity, so a rather large velocity shear is implied by (6). The density and temperature do not change significantly across the discontinuity, but they are fluctuating incoherently throughout the region ($n \approx (29 \pm 2)$ cm^{-3} and $v_T \approx (21 \pm 3)$ km/sec, but v_T tended to be near 19 km/sec ahead of the discontinuity). No periodic variations in the magnetic field direction can be seen.

Finally, consider the peculiar, but not uncommon, sort of wave which is presented in Figure 20. The term wave is not really appropriate because the period is not constant, although it is again on the order of five minutes. Unlike the waves discussed above, the amplitude of the wave is rather large ($\gtrsim 1\gamma$). These "giant undulations" are nested in a filament which is marked by its high u and its low v_T. The field direction does not change appreciably across the discontinuities which define the filament and it does not oscillate in the filament. The density and magnetic field intensity are anticorrelated in the filament, but the data are not sufficiently precise to establish the quantitative relationship.

Theory

Waves were found associated with bulk speed discontinuities in each of the four regions described above. It is natural to attribute the waves to a kind of Kelvin-Helmholtz instability resulting from the relative motion of flux tubes along a glide plane analagous to the motion of the wind on the sea. The stability conditions for such a situation in an incompressible medium are (Landau and Lifshitz, 1960)

$$v \equiv |\vec{v}_2 - \vec{v}_1| < 2\left[\frac{(H_1^2 + H_o^2)/2}{4\pi\rho}\right]^{1/2} \tag{10}$$

$$(\vec{H}_1 \times \vec{H}_2)^2 \geq 2\pi\rho \{(H_1 \times v)^2 + (H_2 \times v)^2\} \tag{11}$$

These conditions show that the magnetic field tends to stabilize the flow when the adjacent flux tubes are not parallel, which explains why velocity discontinuities can exist. Equation (10) shows that the medium becomes unstable when flux tubes try to transport matter at a relative speed which is greater than a quantity which is on the order of the Alfven speed. For the wave on December 22, 1965, it is found that $H_1 \approx 2.5\gamma$, $H_2 \approx 3\gamma$ and $n \approx 30$ cm^{-3}, so (10) predicts that an instability should develop if $v > 20$ km/sec. Equation 7 and the measured Δu give $v > 10$ km/sec which is near the limit of stability, if incompressible hydromagnetic theory is applicable. This suggests that the interplanetary medium is on the verge of instability when B is low and n is high. Under these conditions the medium may become turbulent. It is clear that there is a need for a better theoretical understanding of the physics of gliding flux tubes and complete vector measurements of the bulk velocity.

G. SUMMARY

This report analyzes micro-scale ($\lesssim$ .01 AU) structures which were found in combined interplanetary magnetic field and plasma data obtained by the deep space probe Pioneer 6. The major new results are as follows:

1) Regions exist in the interplanetary medium in which the proton temperature, T, is constant and $B^2 \propto n$. These are interpreted as isothermal, equilibrium regions. From the slope of the B^2 vs n line for each of two regions, it is calculated that the ratio of the electron temperature to the proton temperature is $T_{\perp}'/T_{\perp} \approx 6.5$. This high electron temperature is consistent with the theory of Sturrock and Hartle (1966) and implies that electrons may at times play a dominant role in the dynamics of the interplanetary plasma.

2) Simultaneous discontinuities in the plasma parameters and magnetic field parameters do exist in the interplanetary medium. A classification scheme is presented which identifies thirteen (13) possible types of tangential discontinuities in terms of signatures which describe the changes in B, n and T across a discontinuity. Nine of these signatures were found among the hydromagnetic discontinuities in the Pioneer 6 data.

3) Small discontinuities in the bulk speed, u, often occur simultaneously with discontinuities in n, T and $\vec{B}$. It is shown that this effect would be produced at the spacecraft by the passage of two flux tubes which move relative to one another along a "glide plane" that moves radially from the sun. It is noted that B is very uniform near discontinuities in u. This shows that the interplanetary medium is not everywhere turbulent and it suggests that glide planes may play a fundamental role in reducing stresses in the interplanetary medium.

4) The magnitude of $\vec{B}$ is nearly constant across most of the directional discontinuities discussed by Burlaga and Ness (1967). It is hypothesized that most discontinuities in the interplanetary medium are (000) discontinuities.

5) A D-sheet is shown at a discontinuity in n, u, and T. This is interpreted as a transitional region at a tangential discontinuity as described by Landau and Lifshitz (1960). Plasma data for the D-sheets discussed by Burlaga and Ness (1967) shows that the density is enhanced at the dip in $|\vec{B}|$ in a D-sheet, except when the dip is very small. A significant temperature peak was observed at the dip in $|\vec{B}|$ in only one case; that case was exceptional because of the large amount of magnetic field energy which was "annihilated".

6) Sometimes the interplanetary magnetic field oscillates sinusoidally with an apparent period of approximately five minutes. One case is shown for which the magnetic field vector also rotates, indicating a polarized wave. All of the observed waves are attached to a discontinuity in the bulk speed. It is suggested that these waves are produced by a Kelvin-Helmholtz instability which results when adjacent flux tubes move along a glide plane at a relative speed which is greater than the Alfvén speed. This leads to the hypothesis that turbulence may be observed near large discontinuites in the bulk speed, particularly in regions of low $|\vec{B}|$ and high n.

Acknowledgements

I want to express my sincere thanks to the experimenters who generously made their data available to me. Dr. N. Ness of NASA-Goddard Space Flight Center offered me the Pioneer 6 magnetometer data and suggested that I study discontinuities; I benefited from many discussions with him. Drs. L. Lazarus, H. Bridge and V. Formisano of MIT provided the plasma data, and helped me to understand their plasma probe and data reduction scheme. It is also a pleasure to acknowledge useful discussions with Drs. D. Fairfield, K. Ogilvie, G. Siscoe, and H. Taylor, and the technical support of Mr. R. Bailey. This work was supported by a NAS-NASA Resident Research Associateship.

References

Burlaga, L. F., and N. F. Ness, Macro-Micro Structure of the Interplanetary Magnetic Field, NASA-GSFC Preprint X-612-67-278, June 1967.

Colburn, D. S. and C. P. Sonett, Discontinuities in the Solar Wind, Space Science Reviews, 5, 439-506, 1966.

Coleman, Paul J., Jr., Wave-like Phenomena in the Interplanetary Plasma: Mariner 2, Planet. Space Sci., 15, 953-973, 1967.

Gosling, J. T., J. R. Asbridge, S. J. Bame, A. J. Hundhausen and I. B. Strong, Measurements of the Interplanetary Solar Wind During the Large Geomagnetic Storm of April 17-18, 1965, J. Geophys. Res., 72, 1813-1822, 1967.

Hundhausen, A. J., J. R. Asbridge, S. J. Bame, H. E. Gilbert, and I. B. Strong, Vela 3 Satellite Observations of Solar Wind Ions: A Preliminary Report, J. Geophys. Res., 72, 87-100, 1967.

Landau, L. D., and E. M. Lifshitz, Electrodynamics of Continuous Media, Pergamon Press, New York, 1960.

Lazarus, A. J., H. S. Bridge, and J. Davis, Preliminary Results from the MIT Plasma Experiment, J. Geophys. Res., 71, 3787-3790, 1966.

Mihalov, J. D., C. P. Sonett and D. S. Colburn, On Magnetic Field Reconnection at Tangential Discontinuities in the Solar Wind (to be published).

Ness, N. F., C. S. Scearce and S. Cantarano, Preliminary Results from the Pioneer 6 Magnetic Field Experiment, J. Geophys. Res., 71, 3305-3313, 1966.

Parker, E. N., Interplanetary Dynamical Processes, Interscience Publishers, New York, 1963.

Siscoe, G. L., L. Davis, Jr., P. J. Coleman, Jr., E. J. Smith, and D. E. Jones, Interplanetary Magnetic Field Power Spectra and Discontinuities Based on Mariner 4 Data, (to be published).

Sturrock, P. A., and R. E. Hartle, Two-Fluid Model of the Solar Wind, Physical Rev. Letters, 16, 628-631, 1966.

TABLE 1 This gives 13 possible signatures of a tangential discontinuity and arranges them in three classes. Class T0 contains only a directional discontinuity. Classes T2 and T3 contain the permutations and reflections of (+ - 0) and (+ - +) respectively.

TABLE 2 Plasma parameters for four D-sheets. "Before" and "After" refer to averages of the parameters ten minutes before and ten minutes after the directional discontinuity. "At" gives the value of the parameters at a time very near to the time of the discontinuity. The angle ω is the angle between the magnetic field vectors on either side of the discontinuity.

TABLE 1

TANGENTIAL DISCONTINUITIES

T0	(0 0 0)*		
T2	(+ - 0)* (- + 0)*	(0 + -)* (0 - +)	(- 0 +)* (+ 0 -)*
T3	(+ - +)* (- + -)*	(+ + -)* (- - +)	(- + +) (+ - -)

*Observed in Pioneer 6 data

TABLE 2

		u (km/sec)			n (cm^{-3})			v_T (km/sec)		
Day/hour	ω	Before	At	After	Before	At	After	Before	At	After
352/4	119°	321 ± 3	328 ± 2	326 ± 2	5.7	7.0	5.9	21 ± 2	18 ± 2	19 ± 2
354/6	150°	413 ± 3	394 ± 5	393 ± 5	4.0	5.0	4.3	28 ± 4	33 ± 5	32 ± 5
361/10	85°	561 ±6	613 ± 9	589 ± 6	3.1	3.0	3.0	48 ± 7	53 ± 7	47 ± 6
25/10	130°	594 ± 8	596 ± 10	596 ± 7	2.4	3.0	2.4	54 ± 9	60 ± 6	48 ± 6

FIGURE CAPTIONS

Figure 1 A cascade of (- + 0) discontinuities in an equilibrium region. (see text).

Figure 2 This shows that $B^2 \propto n$ in the segment shown in Figure 1. Thus, the segment satisfies one necessary condition for an equilibrium region. It is possible to estimate the electron temperature from the slope of this line if the region is isothermal.

Figure 3 A cascade of (+ - 0) discontinuities in an equilibrium region. This is the complement of the segment shown in Figure 1.

Figure 4 A plot showing that $B^2 \propto n$ in the segment described in Figure 3.

Figure 5 A schematic illustration which describes a tangential discontinuity in terms of two hypothetical, infinitesimal, rectangular, magnetic flux tubes. The figure shows the special case when the flux tubes are mutually perpendicular and are inclined at an angle θ with respect to the ecliptic plane.

Figure 6 Another illustration of a tangential discontinuity. This is complementary to Figure 5 in that an element of the surface of the discontinuity (the glide plane) is shown (assuming a real discontinuity - no rotation fan) but the flux tubes are not shown. The arrows indicate that the flux tubes are moving relative to the glide plane with velocities $\vec{v}_1$ and $\vec{v}_2$. The glide plane moves away from the sun with the plasma bulk velocity $\vec{u}$.

Figure 7 A segment of a region containing a (- 0 +) discontinuity and its complement, a (+ 0 -). Two discontinuity filaments are also shown.

Figure 8 Two directional discontinuities. The one on the left has the signature (0 0 0). The other has the signature (0 + -).

Figure 9 A (+ + -) discontinuity.

Figure 10 A (- + -) discontinuity and its complement, a (+ - +) discontinuity. They combine to form a filament that separates two distinct regions.

Figure 11 This histogram shows that the fractional change of the magnitude of the interplanetary magnetic field across a directional discontinuity is usually near zero.

Figure 12 Illustrations of the magnetic field annihilation hypothesis. The vectors $\vec{B}_1$ and $\vec{B}_2$ specify the magnetic field on the two sides of a directional discontinuity. Each vector is resolved into the components $\vec{A} + B_{min}$. At the discontinuity, $\vec{B}_1$ and $\vec{B}_2$ are superimposed so the A components cancel leaving B_{min} continuous across the discontinuity.

Figure 13 A D-sheet at a plasma discontinuity. It is suggested that the dip in $|\vec{B}|$ marks a transitional region associated with a tangential discontinuity as described by Landau and Lifshitz (1960).

Figure 14 A D-sheet for which the decrease in magnetic pressure is accompanied by an increased plasma density and temperature.

Figure 15 Periodic variations in the interplanetary magnetic field intensity. Note that the wave is nested among a series of discontinuities in the bulk speed and magnetic field direction.

Figure 16 Another view of the wave in the interplanetary magnetic field intensity which was observed on 1/5/66 (see text).

Figure 17 Another wave in the interplanetary magnetic field intensity. Note the oscillations of the magnetic field direction in the filament between 0140 and 0151.

Figure 18 This shows that the magnetic field vector in the filament in Figure 17 was rotating systematically about the observation point between 0142 and 0151, indicating that the wave was polarized.

Figure 19 A D-sheet at a discontinuity in bulk speed which is followed by a large amplitude, nearly periodic variation in the magnetic field intensity.

Figure 20 Large amplitude, non-periodic variations in magnetic field intensity and proton density, nested in a filament which is characterized by a lower thermal speed and a higher bulk speed than surrounding regions.

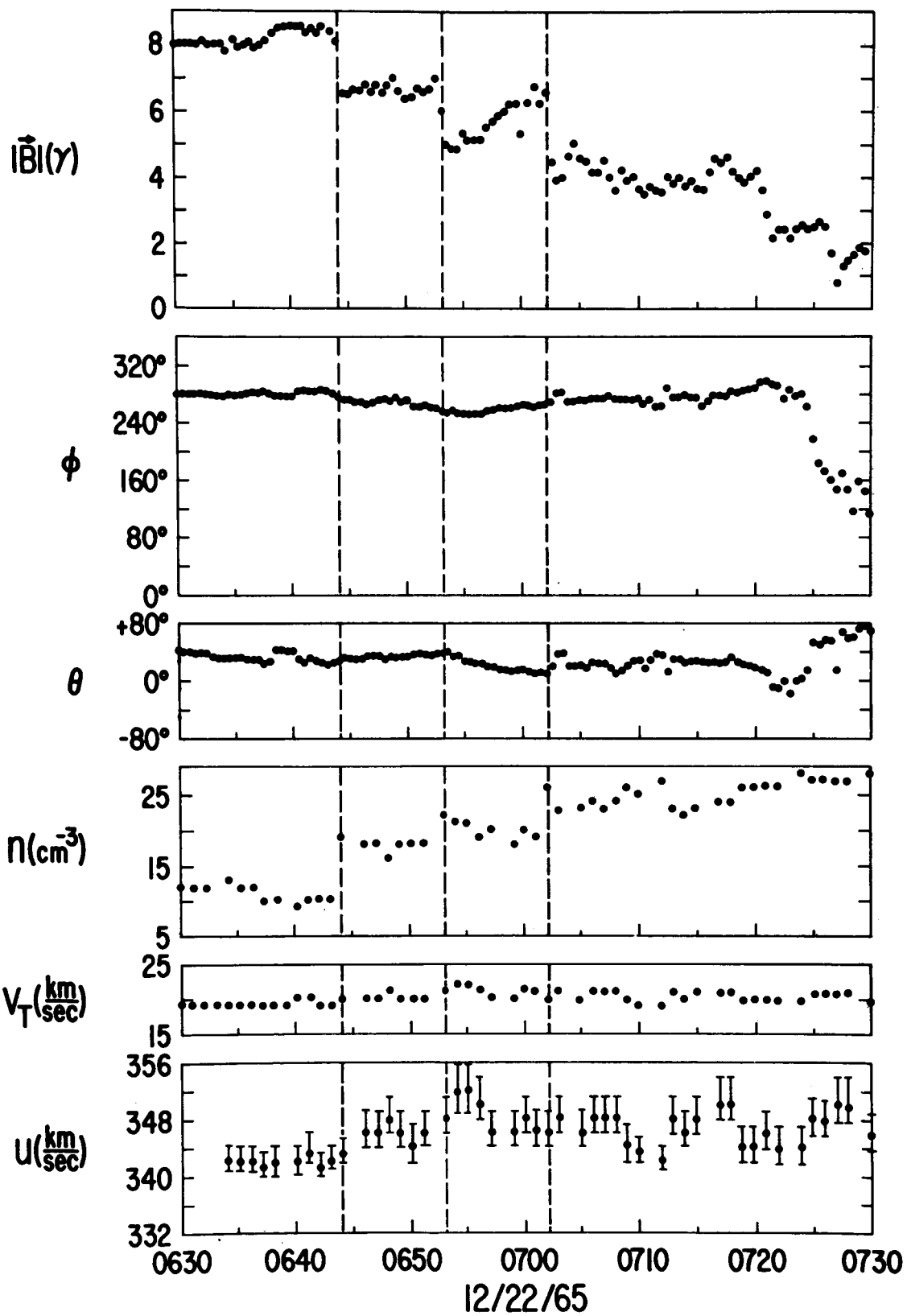
|B|(γ)
8
6
4
2
0
φ
320°
240°
160°
80°
0°
θ
+80°
0°
-80°
n(cm⁻³)
25
15
5
V_T(km/sec)
25
15
U(km/sec)
356
348
340
332
0630
0640
0650
0700
0710
0720
0730
12/22/65

FIGURE 1

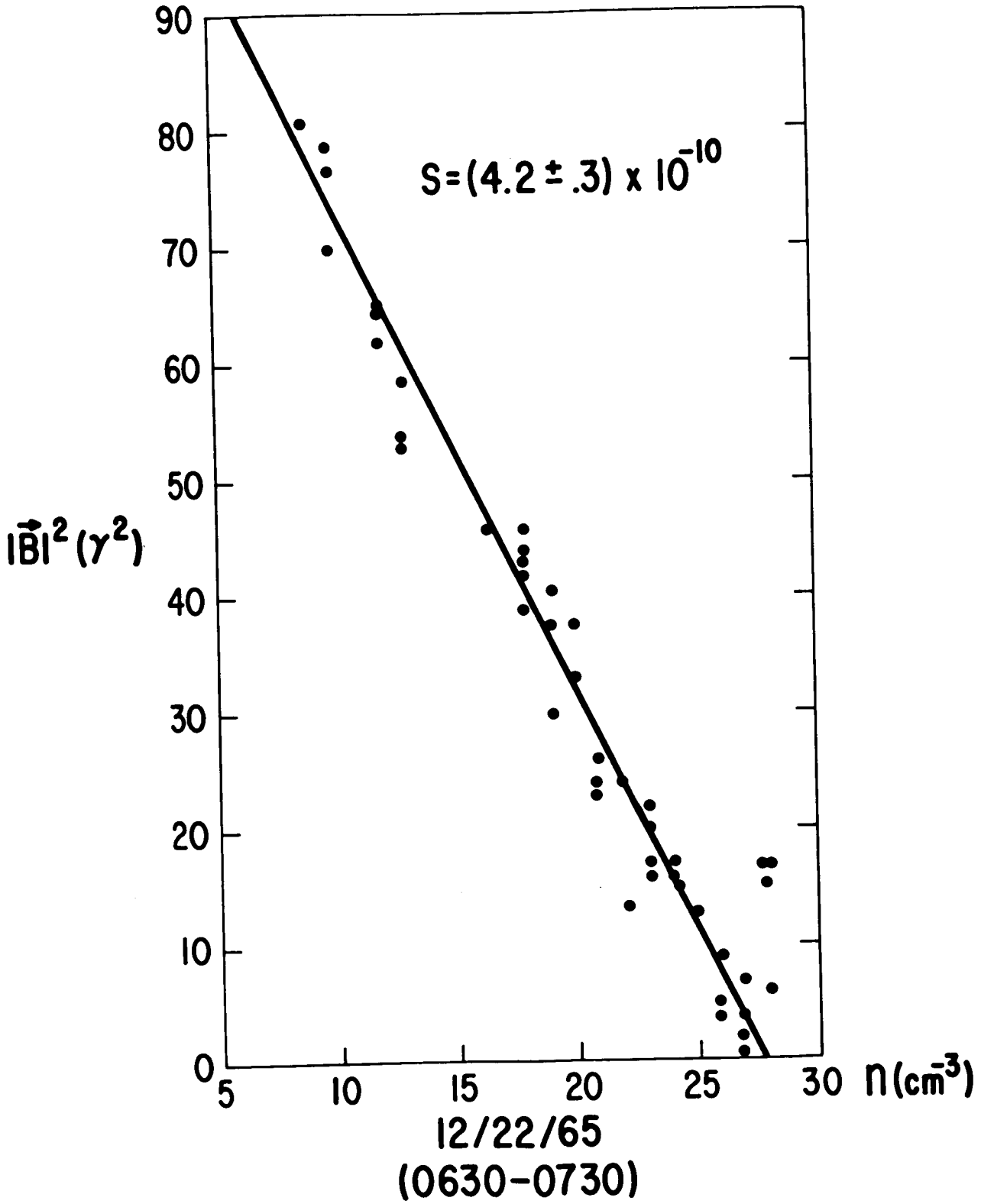
90
80
70
60
50
40
30
20
10
0
5
10
15
20
25
30
$S=(4.2\pm.3)\times10^{-10}$
$|\vec{B}|^2(\gamma^2)$
$n(cm^{-3})$
12/22/65
(0630-0730)

FIGURE 2

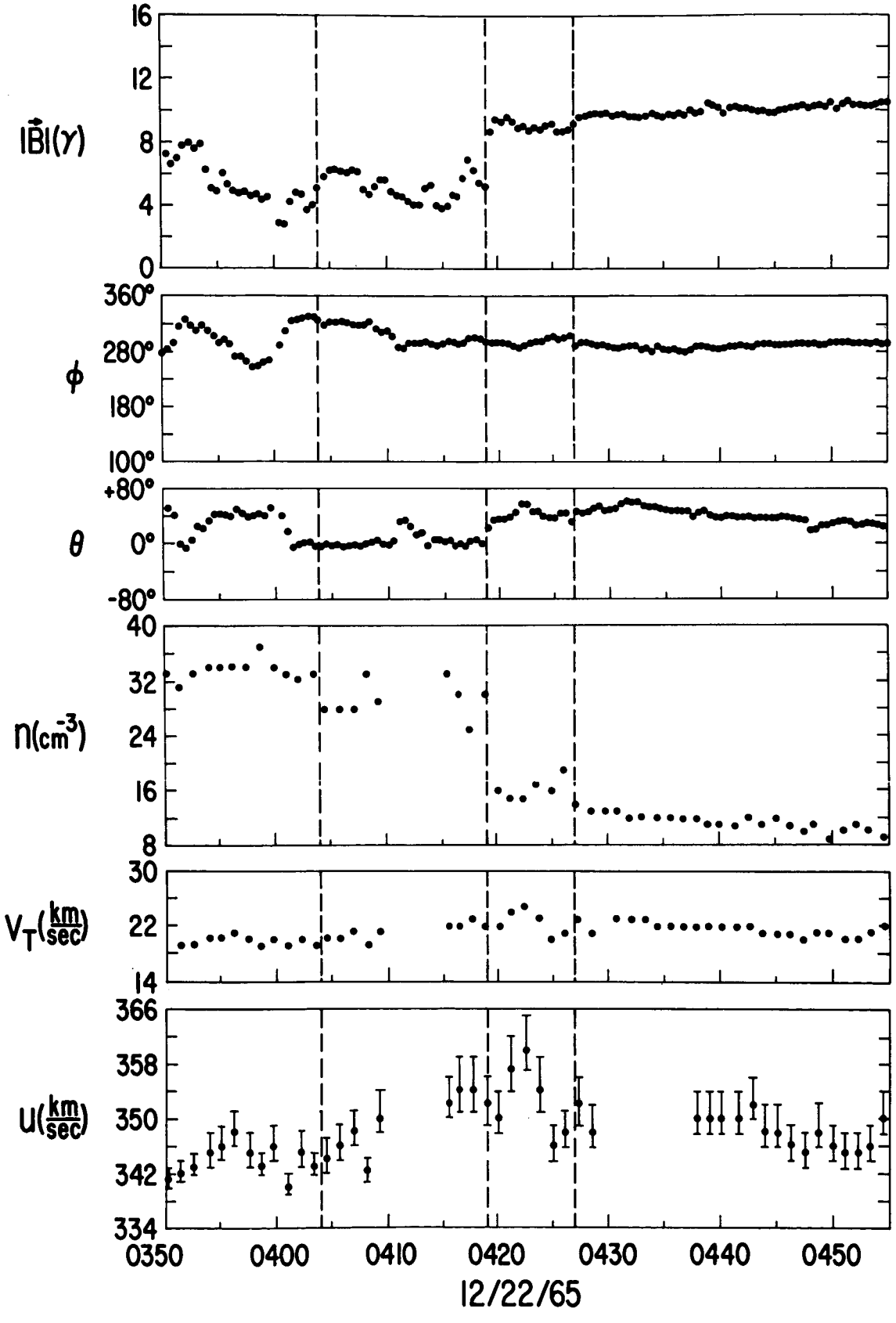
16
12
8
4
0
|B|(γ)
360°
280°
180°
100°
φ
+80°
0°
-80°
θ
40
32
24
16
8
n(cm⁻³)
30
22
14
V_T(km/sec)
366
358
350
342
334
u(km/sec)
0350
0400
0410
0420
0430
0440
0450
12/22/65

FIGURE 3

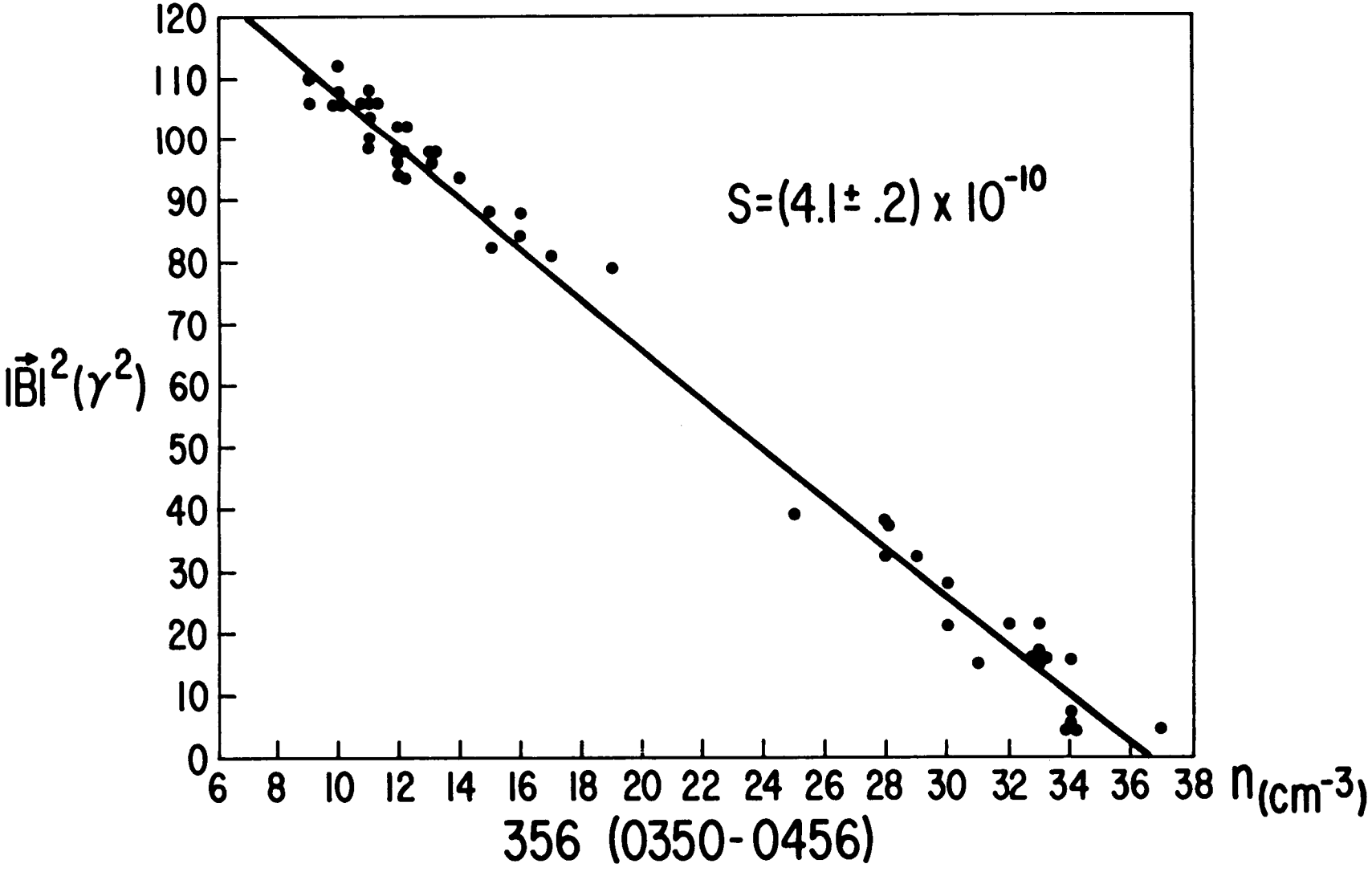
120
110
100
90
80
70
60
50
40
30
20
10
0
$|\vec{B}|^2(\gamma^2)$
$S=(4.1\pm .2)\times 10^{-10}$
6 8 10 12 14 16 18 20 22 24 26 28 30 32 34 36 38 $n_{(cm^{-3})}$
356 (0350-0456)

FIGURE 4

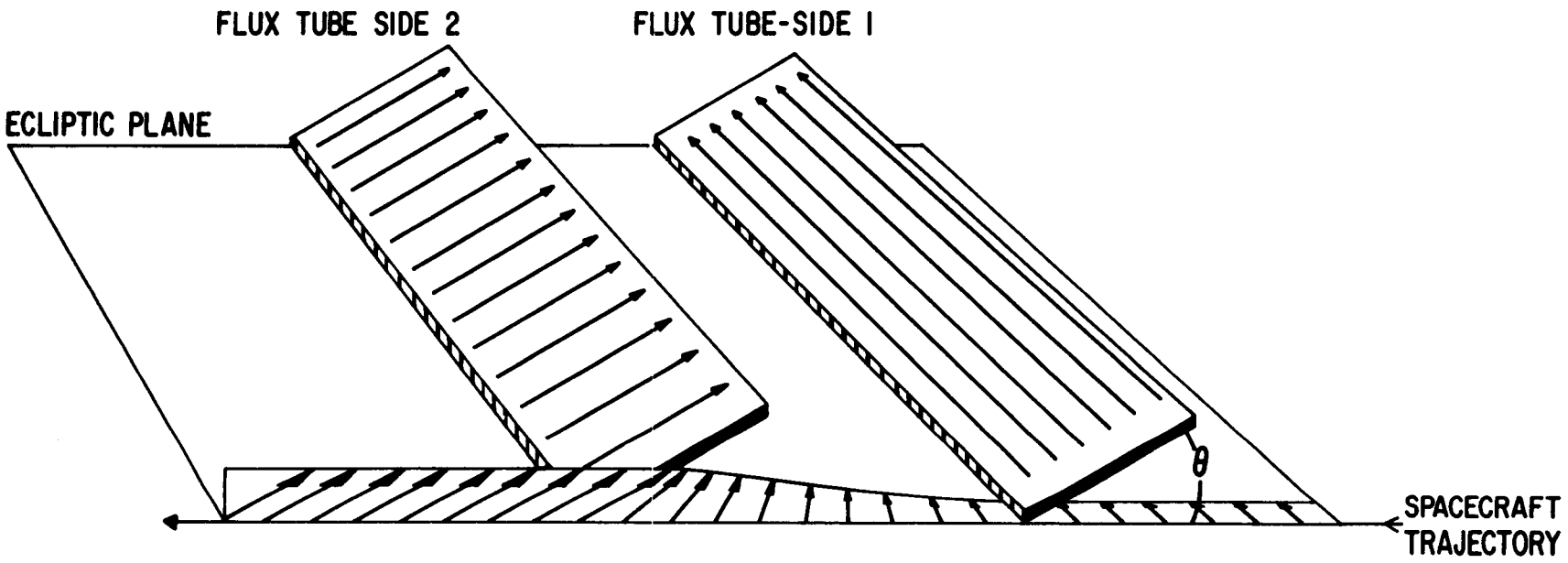

TANGENTIAL DISCONTINUITY

FIGURE 5

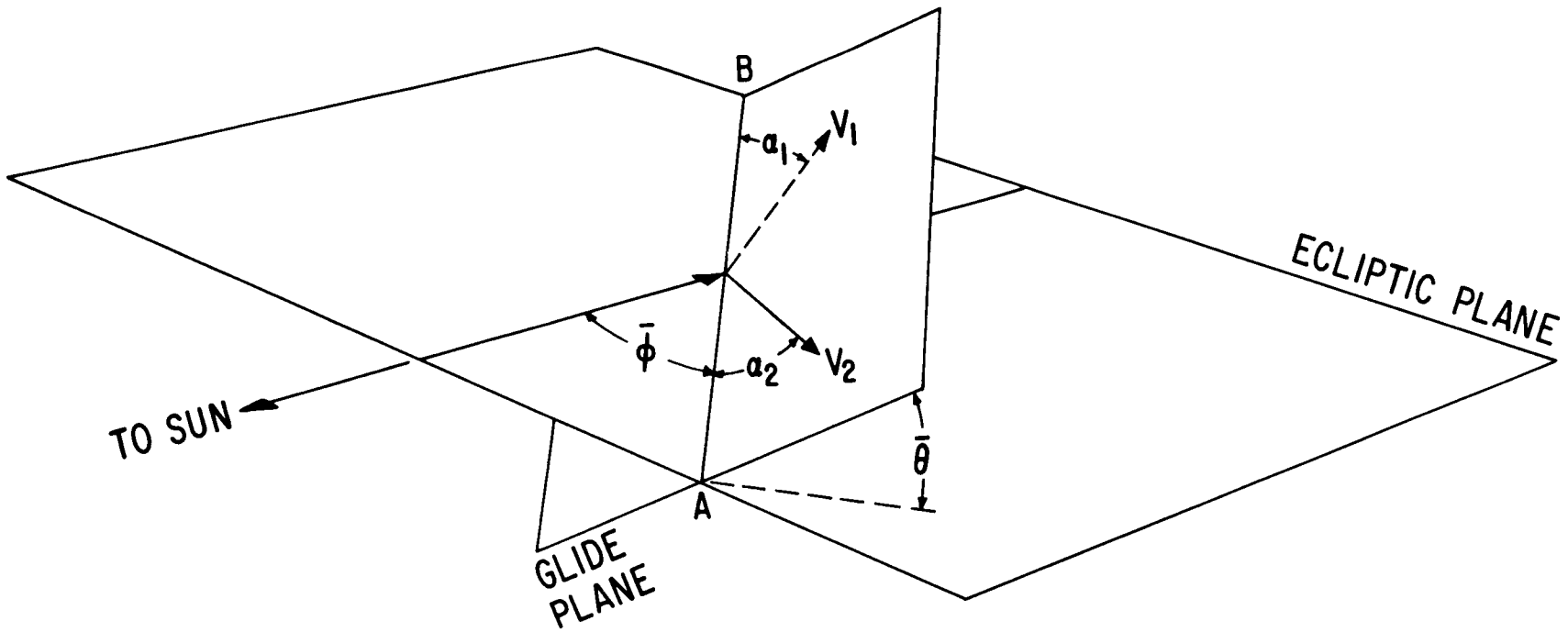
B
a_1
V_1
ECLIPTIC PLANE
$\bar{\phi}$
a_2
V_2
TO SUN
$\bar{\theta}$
A
GLIDE
PLANE

FIGURE 6

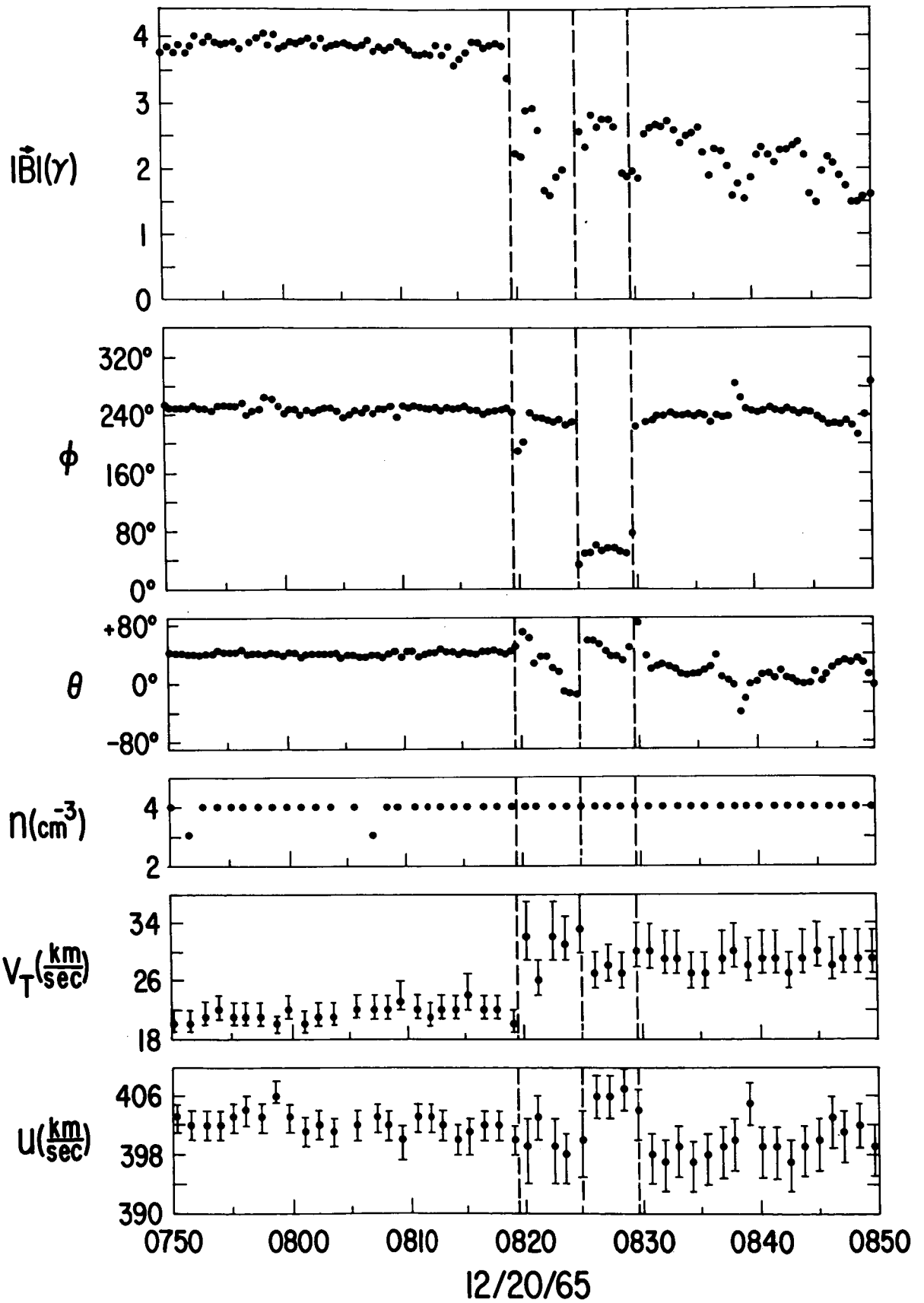
|B̃|(γ)
4
3
2
1
0
φ
320°
240°
160°
80°
0°
θ
+80°
0°
-80°
n(cm⁻³)
4
2
V_T(km/sec)
34
26
18
U(km/sec)
406
398
390
0750
0800
0810
0820
0830
0840
0850
12/20/65

FIGURE 7

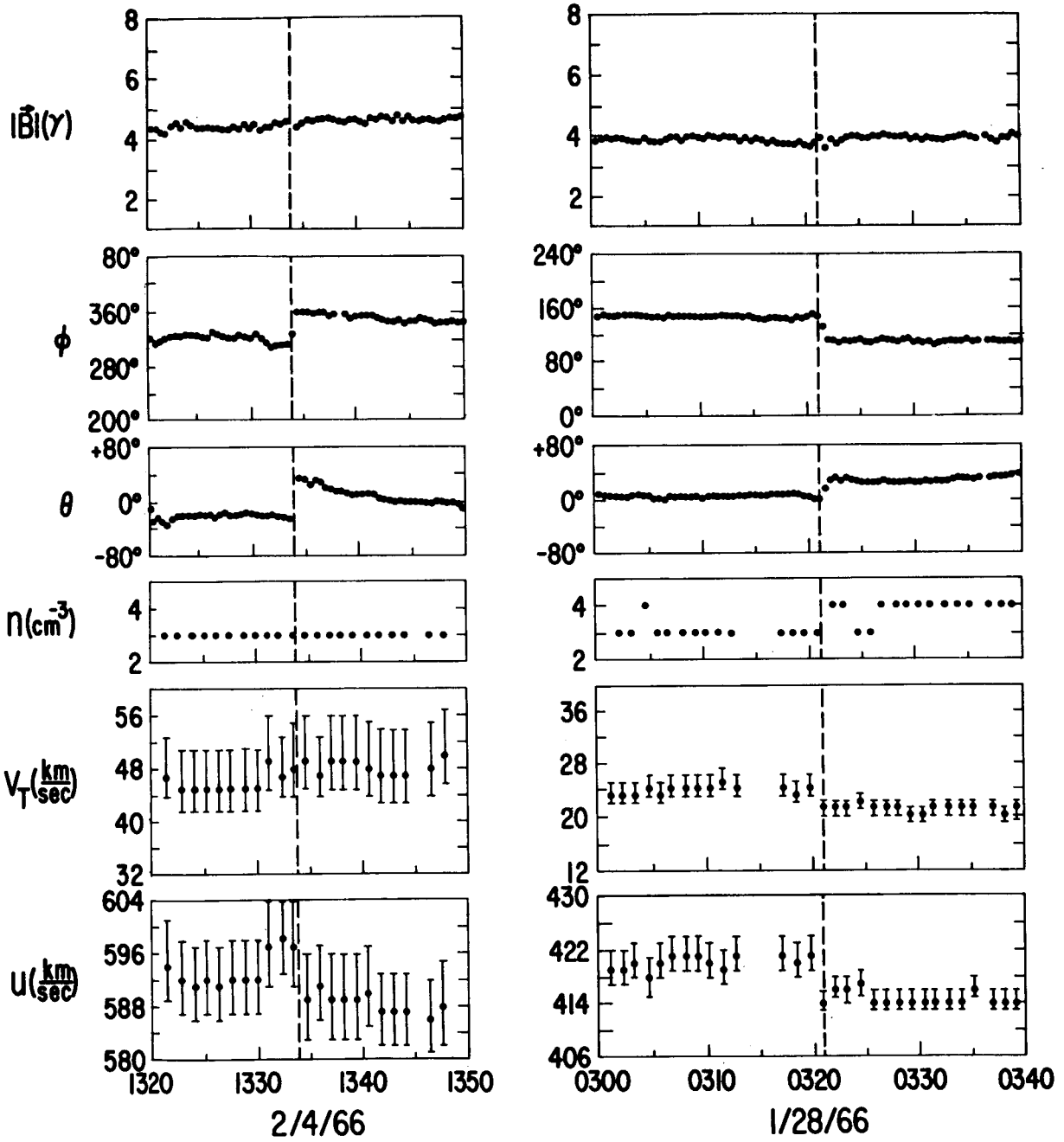
|B|(γ)
φ
θ
n(cm⁻³)
V_T(km/sec)
U(km/sec)
8
6
4
2
80°
360°
280°
200°
+80°
0°
-80°
4
2
56
48
40
32
604
596
588
580
1320
1330
1340
1350
2/4/66
240°
160°
80°
0°
+80°
0°
-80°
4
2
36
28
20
12
430
422
414
406
0300
0310
0320
0330
0340
1/28/66

FIGURE 8

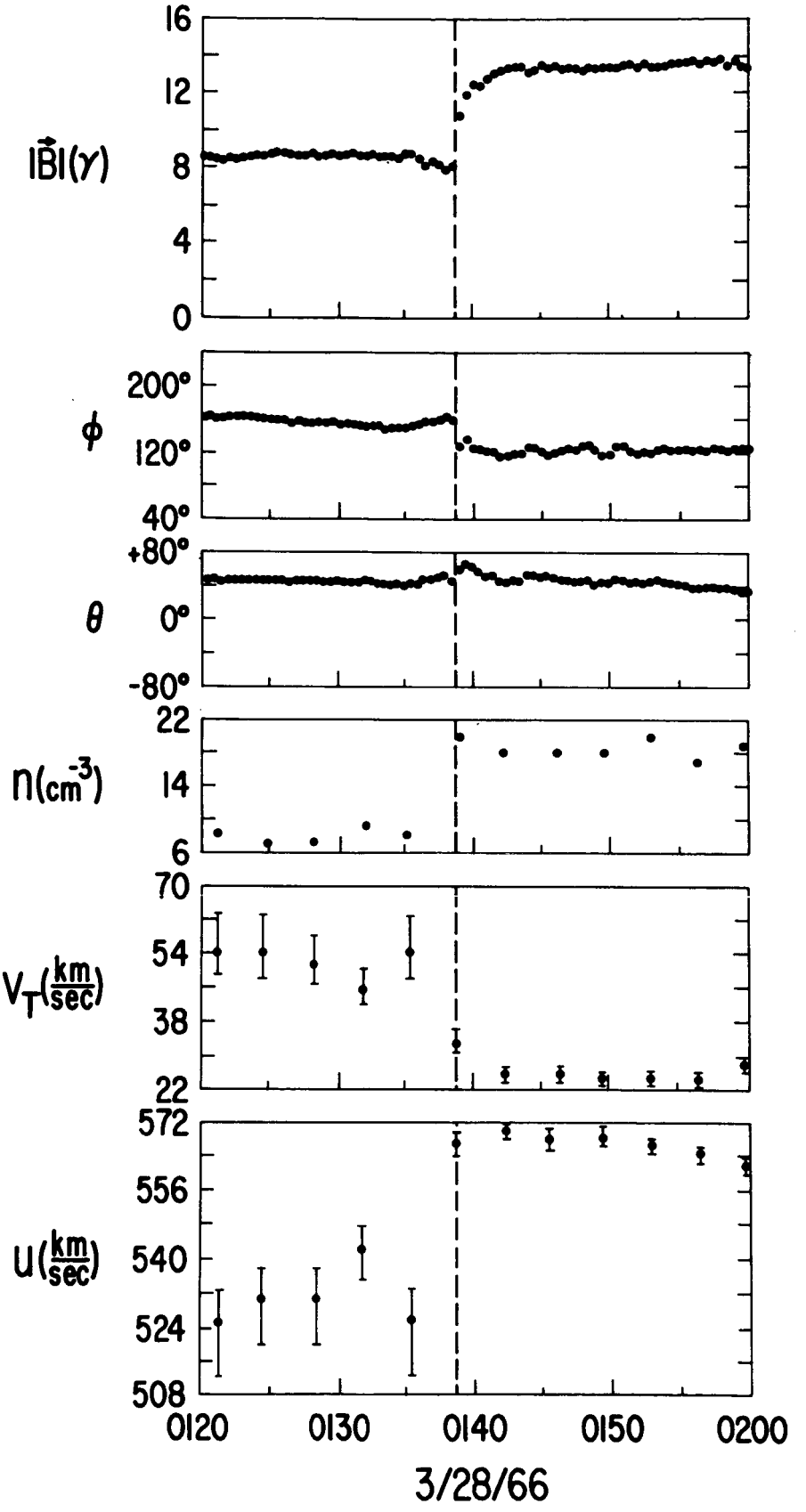
16
12
8
4
0
|B|(γ)
200°
120°
40°
φ
+80°
0°
-80°
θ
22
14
6
n(cm⁻³)
70
54
38
22
V_T(km/sec)
572
556
540
524
508
U(km/sec)
0120
0130
0140
0150
0200
3/28/66

FIGURE 9

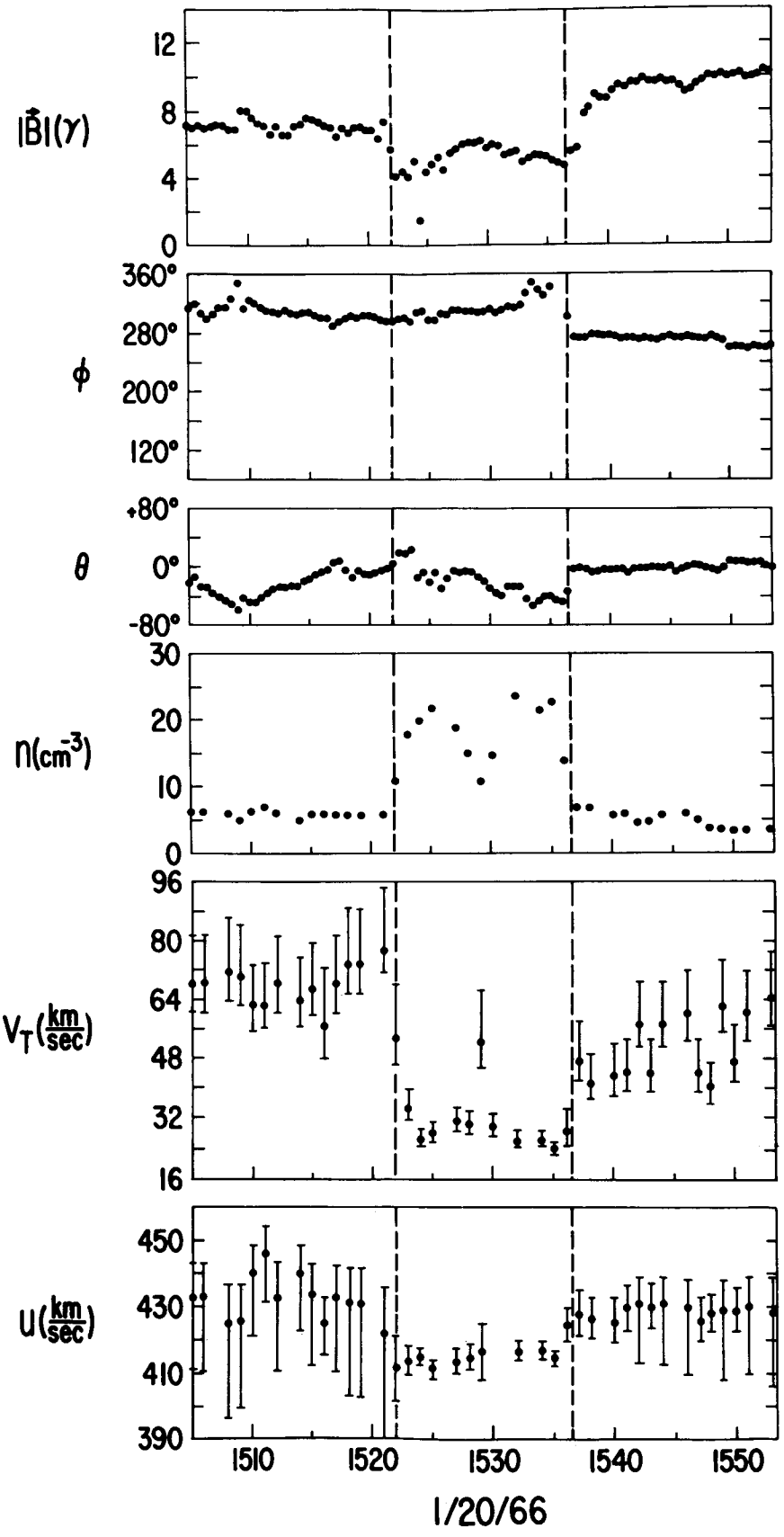
|B|(γ)
12
8
4
0
φ
360°
280°
200°
120°
θ
+80°
0°
-80°
n(cm⁻³)
30
20
10
0
V_T(km/sec)
96
80
64
48
32
16
U(km/sec)
450
430
410
390
1510
1520
1530
1540
1550
1/20/66

FIGURE 10

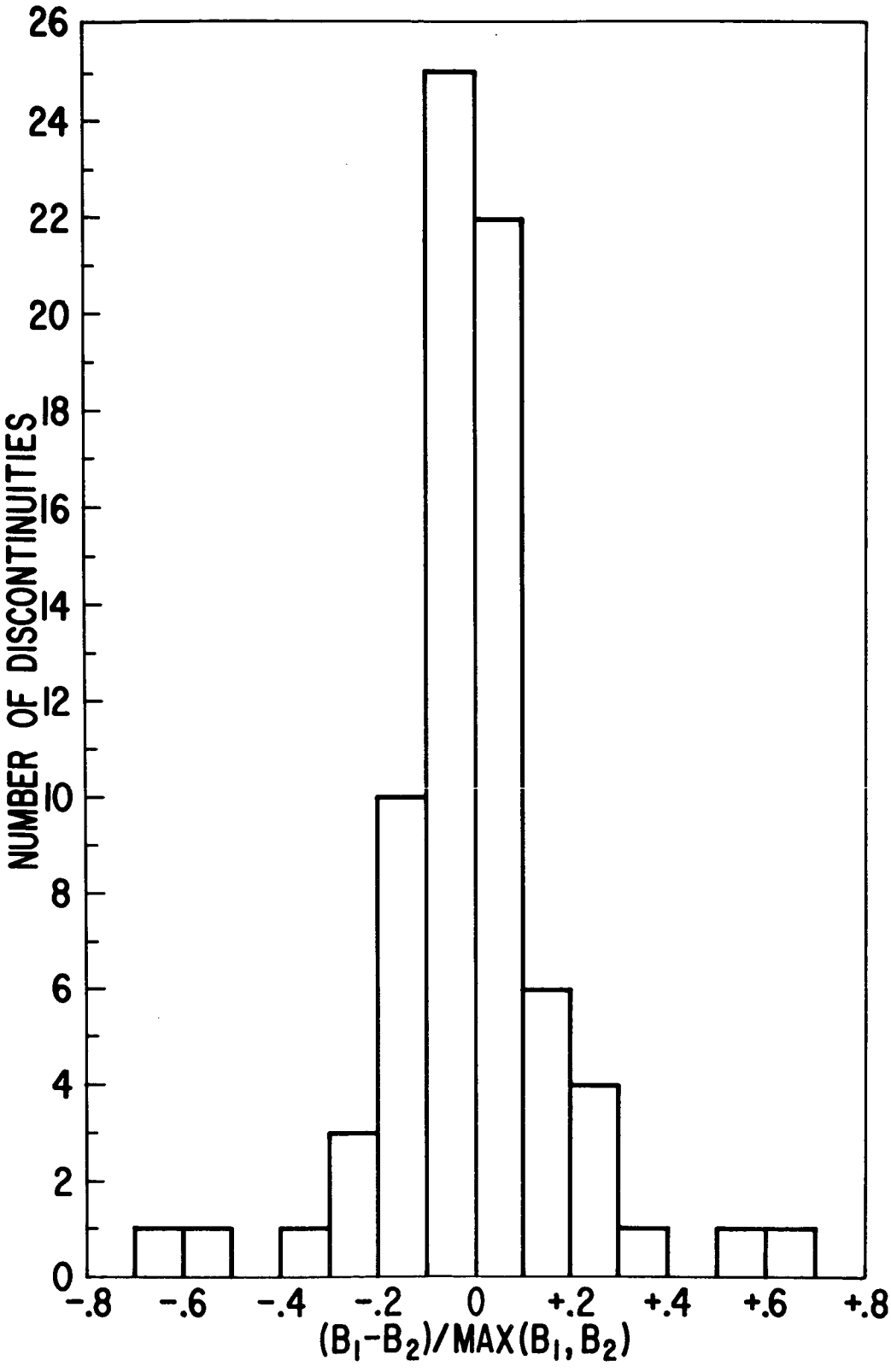
26
24
22
20
18
16
14
12
10
8
6
4
2
0
NUMBER OF DISCONTINUITIES
-.8
-.6
-.4
-.2
0
+.2
+.4
+.6
+.8
(B1-B2)/MAX(B1, B2)

FIGURE 11

$|\vec{B}_1| = |\vec{B}_2| \equiv B$

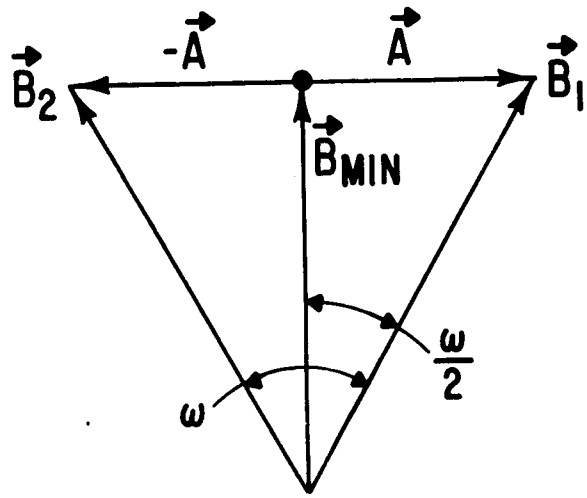

$$\frac{B_{MIN}}{B} = \cos\left(\frac{\omega}{2}\right)$$

$|\vec{B}_1| \neq |\vec{B}_2|$

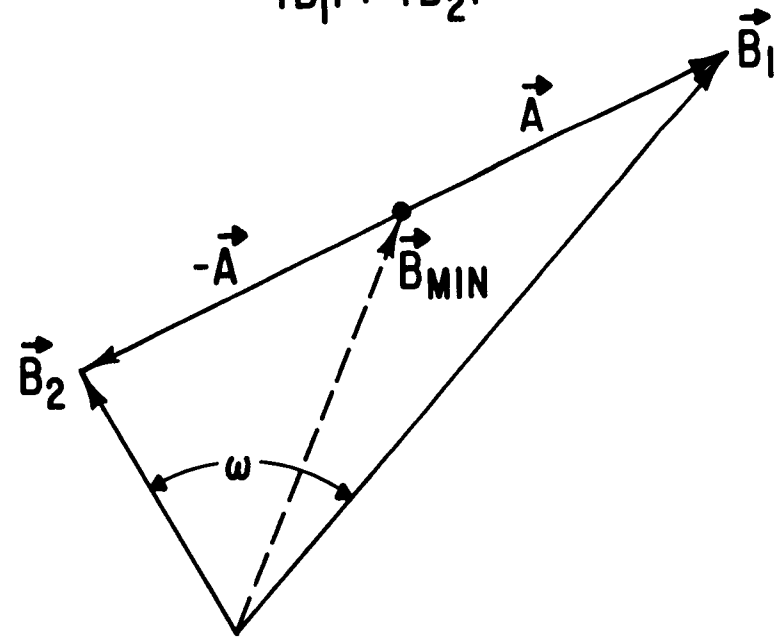

$$4B_{MIN}^2 = B_1^2 + B_2^2 + 2B_1B_2\cos(\omega)$$

FIGURE 12

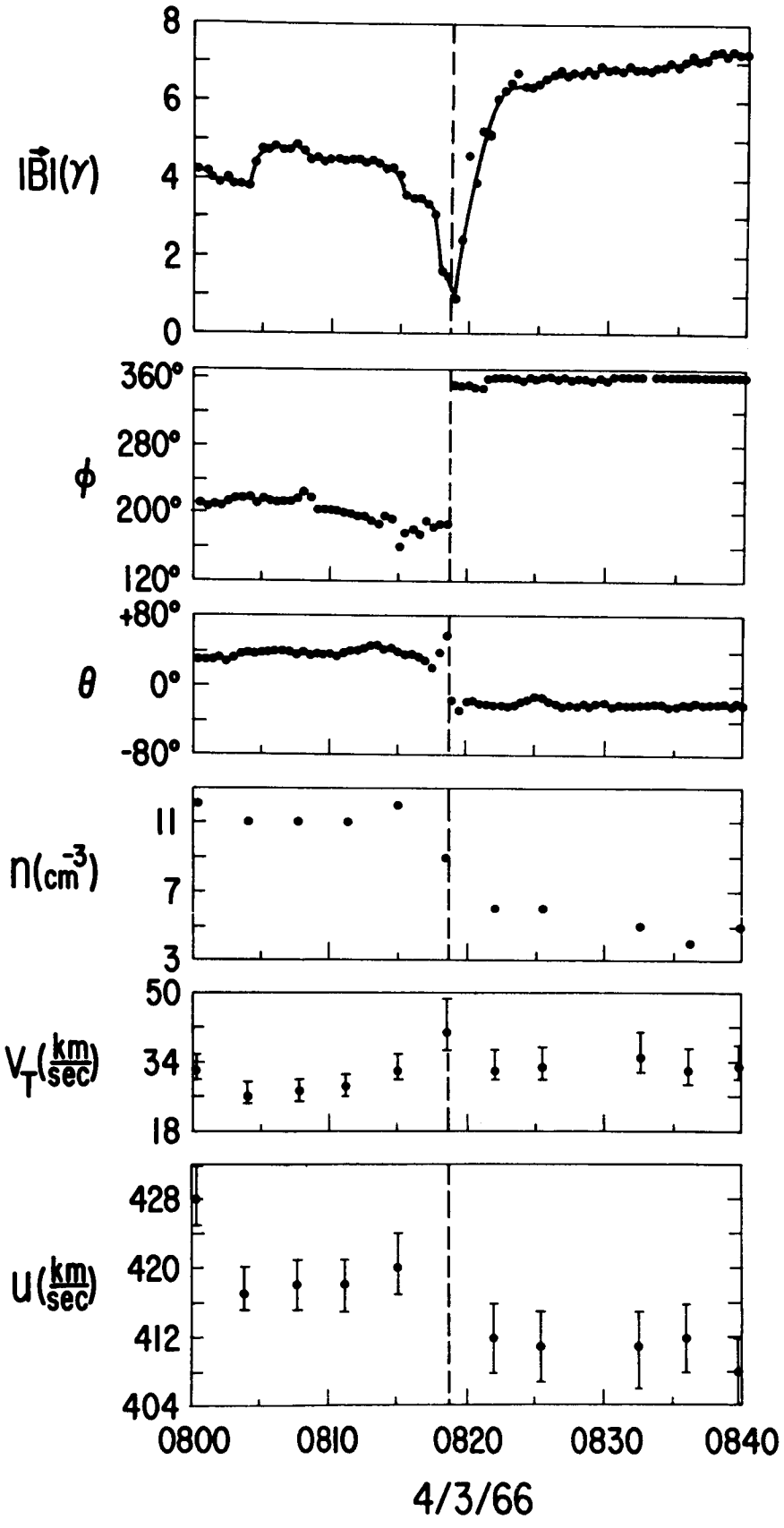
8
6
4
2
0
|B|(γ)
360°
280°
200°
120°
φ
+80°
0°
-80°
θ
11
7
3
n(cm⁻³)
50
34
18
V_T(km/sec)
428
420
412
404
U(km/sec)
0800
0810
0820
0830
0840
4/3/66

FIGURE 13

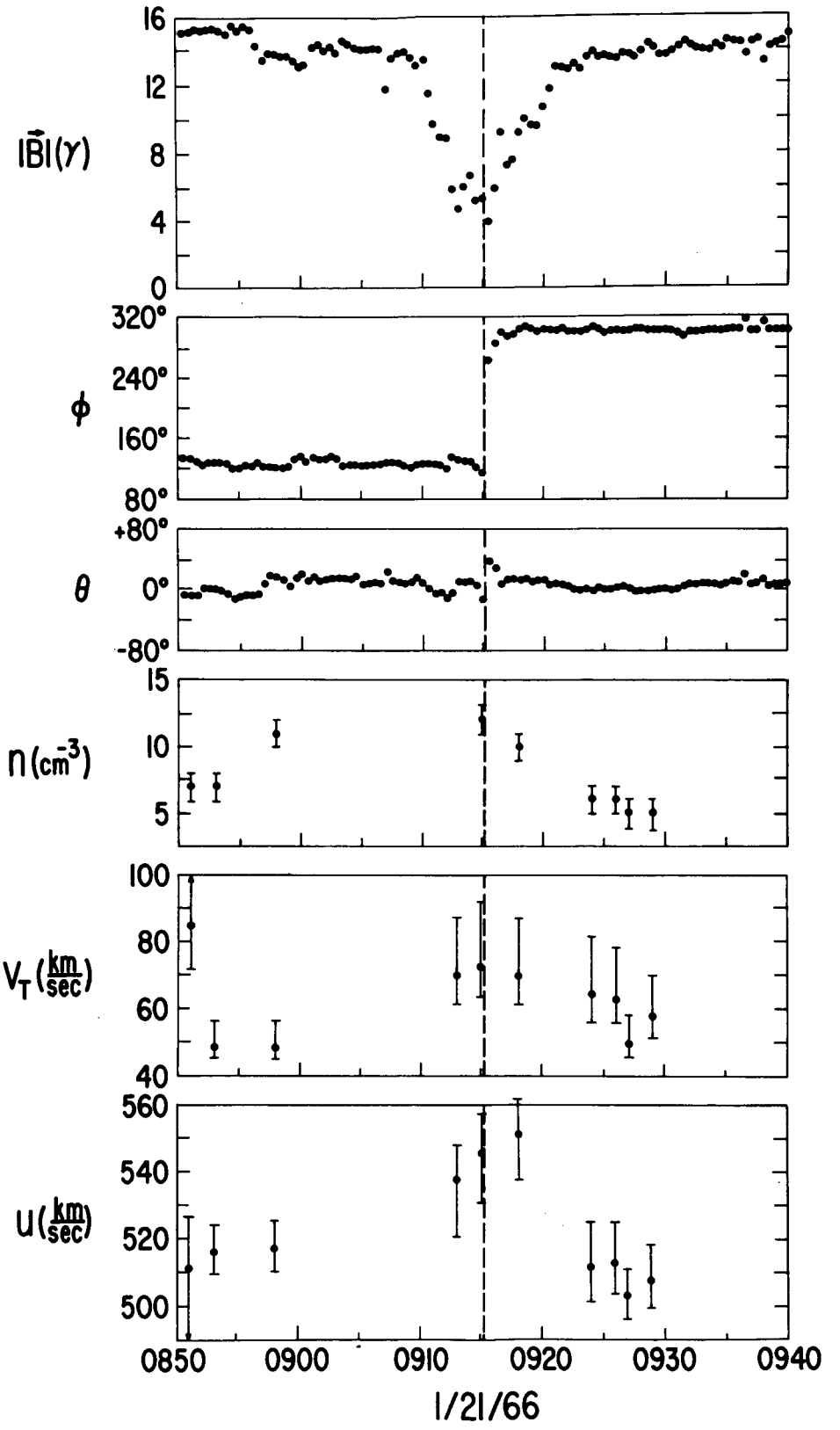
16
12
8
4
0
|B⃗|(γ)
320°
240°
160°
80°
φ
+80°
0°
-80°
θ
15
10
5
n(cm⁻³)
100
80
60
40
V_T (km/sec)
560
540
520
500
U (km/sec)
0850
0900
0910
0920
0930
0940
1/21/66

FIGURE 14

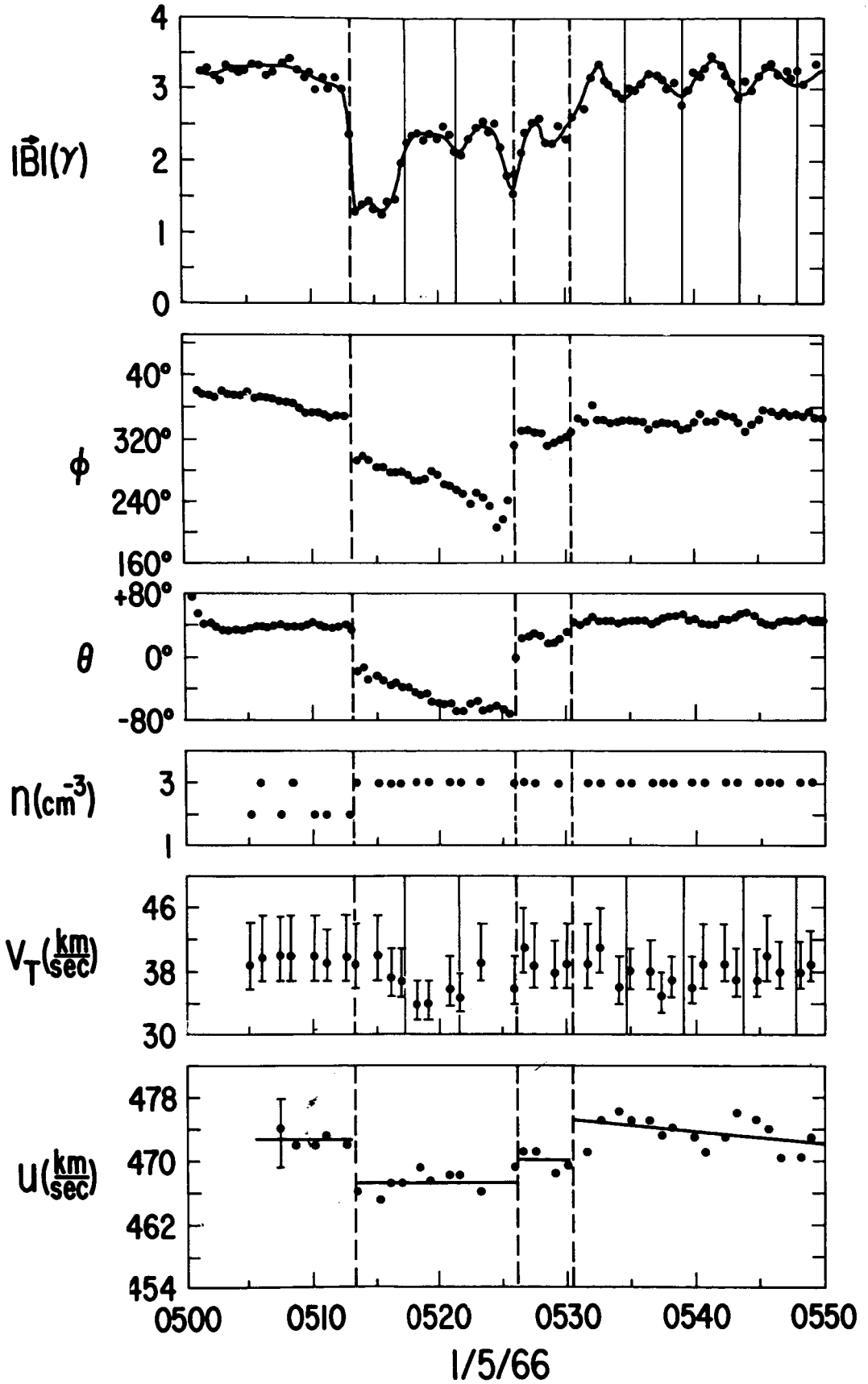
|B|(γ)
4
3
2
1
0
φ
40°
320°
240°
160°
θ
+80°
0°
-80°
n(cm⁻³)
3
1
V_T(km/sec)
46
38
30
U(km/sec)
478
470
462
454
0500
0510
0520
0530
0540
0550
1/5/66

FIGURE 15

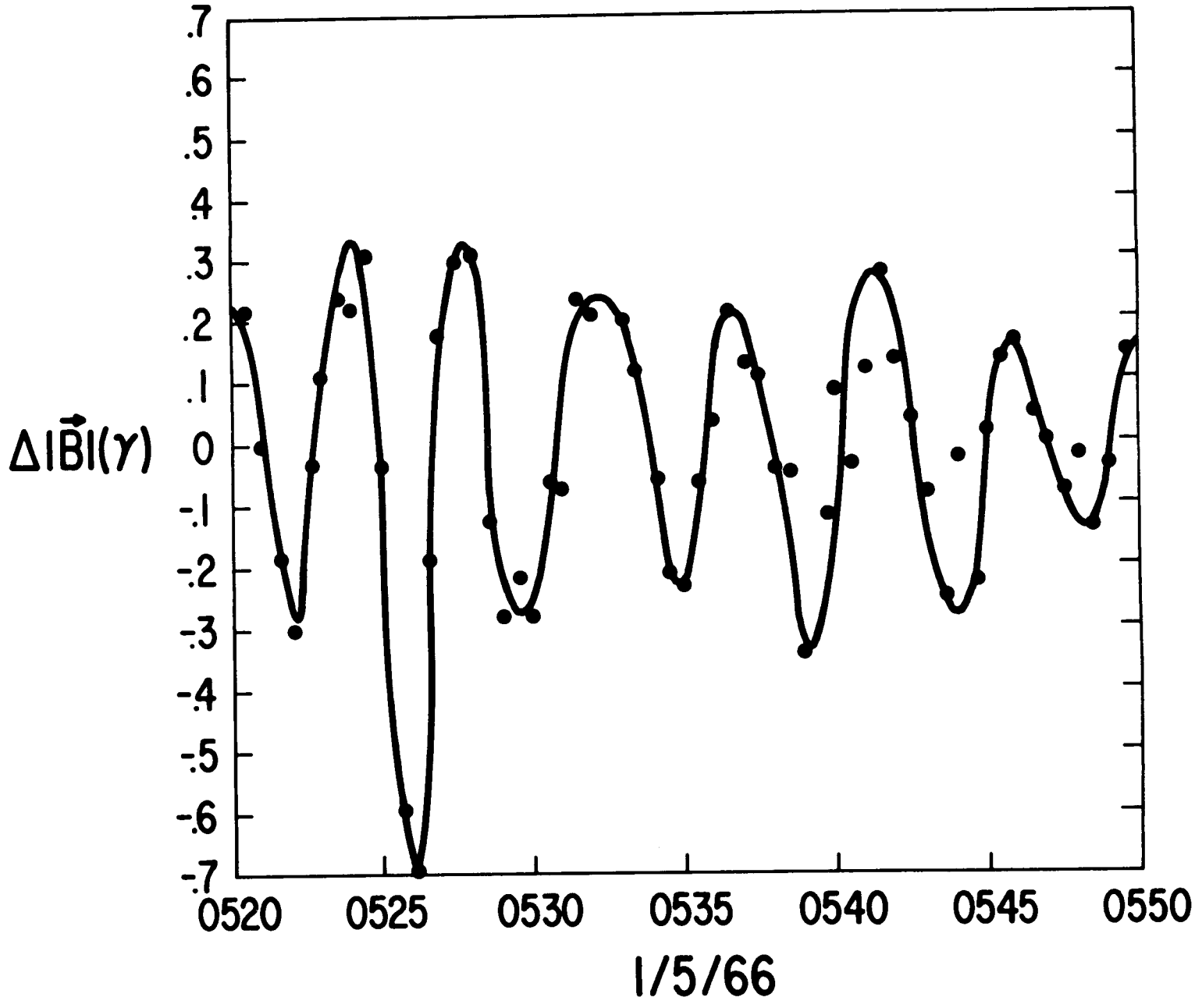
.7
.6
.5
.4
.3
.2
.1
0
-.1
-.2
-.3
-.4
-.5
-.6
-.7
ΔIB⃗I(γ)
0520
0525
0530
0535
0540
0545
0550
1/5/66

FIGURE 16

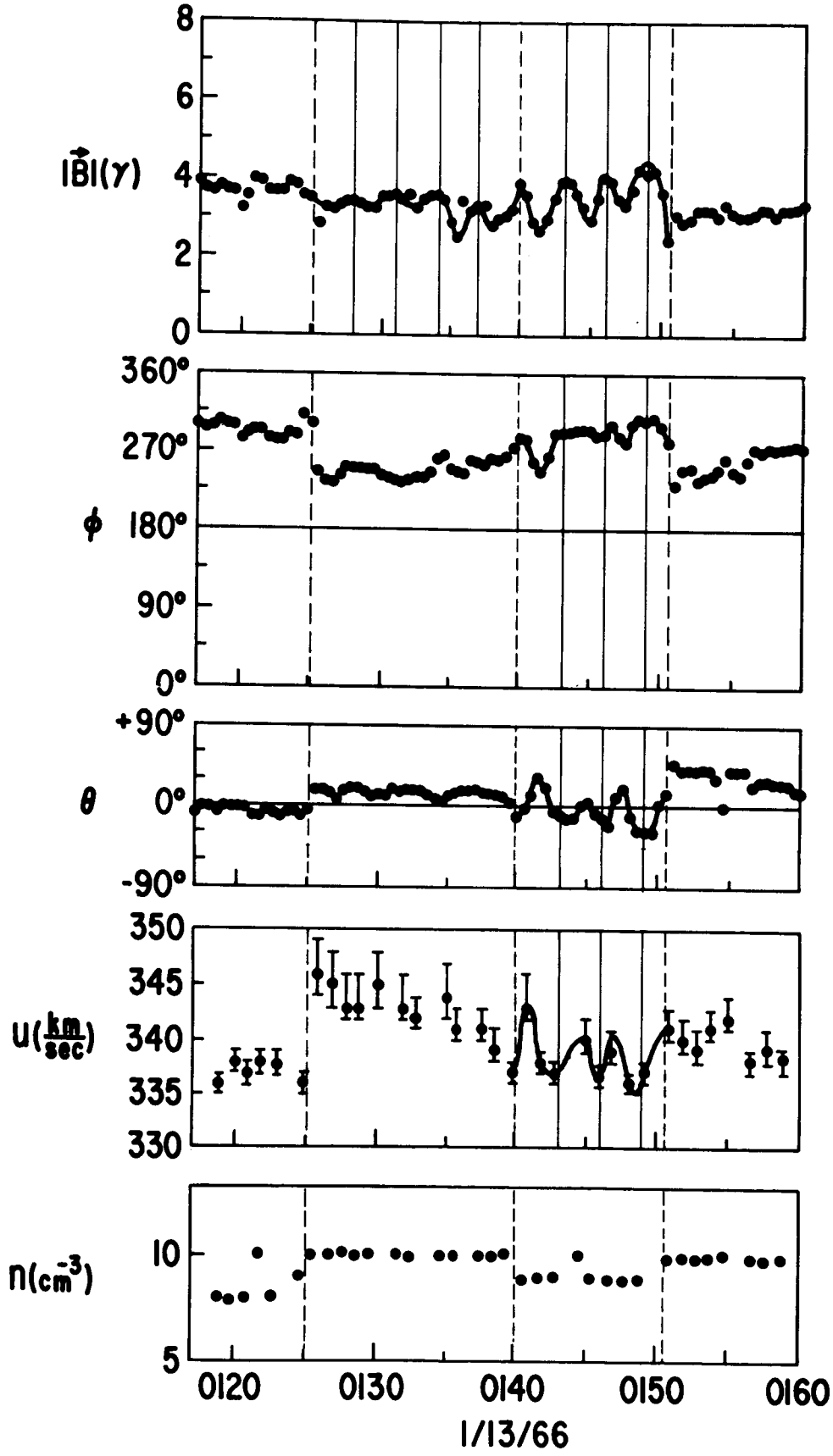
8
6
4
2
0
|B|(γ)
360°
270°
180°
90°
0°
φ
+90°
0°
-90°
θ
350
345
340
335
330
U(km/sec)
10
5
n(cm⁻³)
0120
0130
0140
0150
0160
1/13/66

FIGURE 17

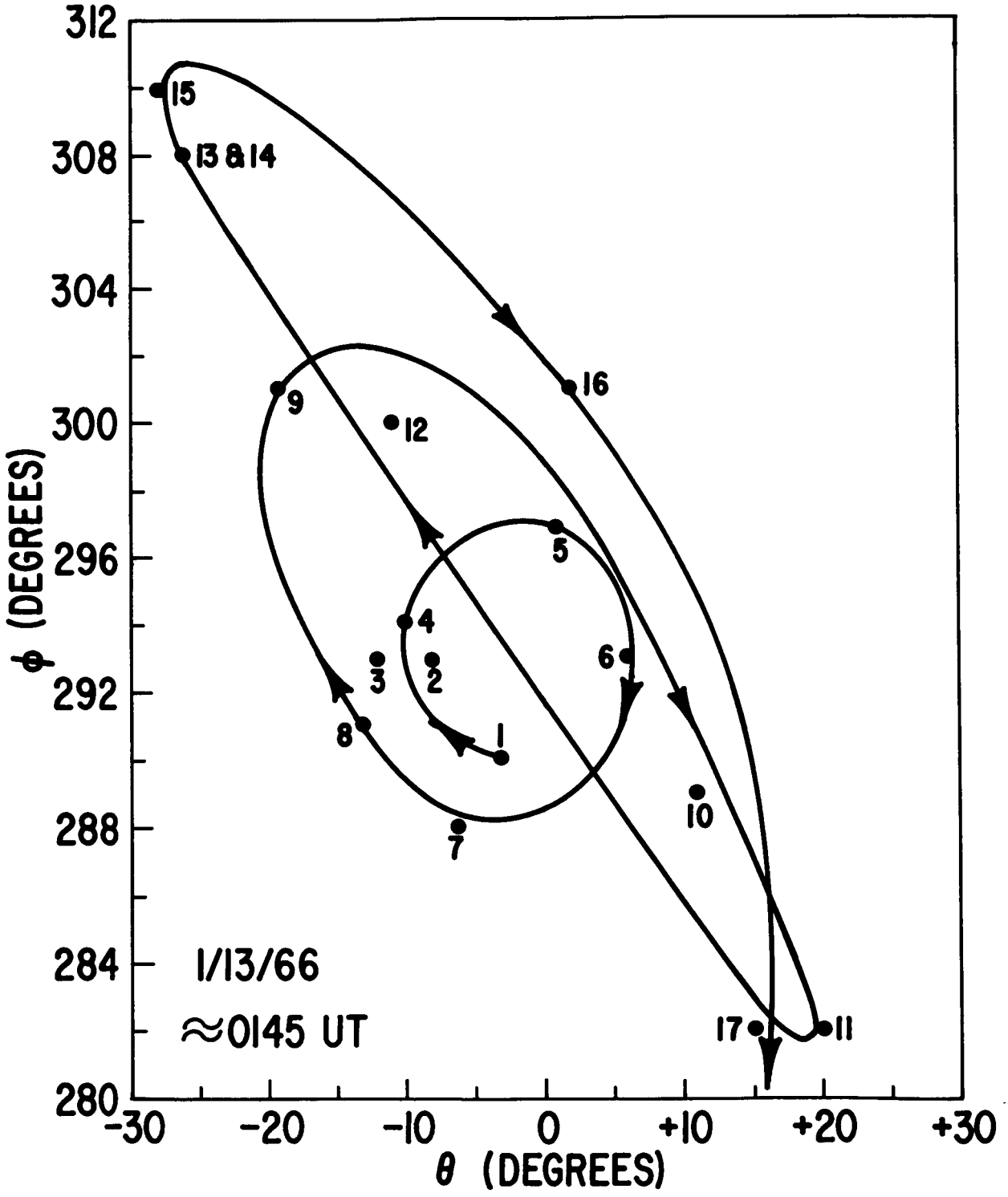
312
308
304
300
296
292
288
284
280
φ (DEGREES)
-30
-20
-10
0
+10
+20
+30
θ (DEGREES)
15
13 & 14
16
9
12
5
4
3
2
6
8
1
7
10
17
11
1/13/66
≈0145 UT

FIGURE 18

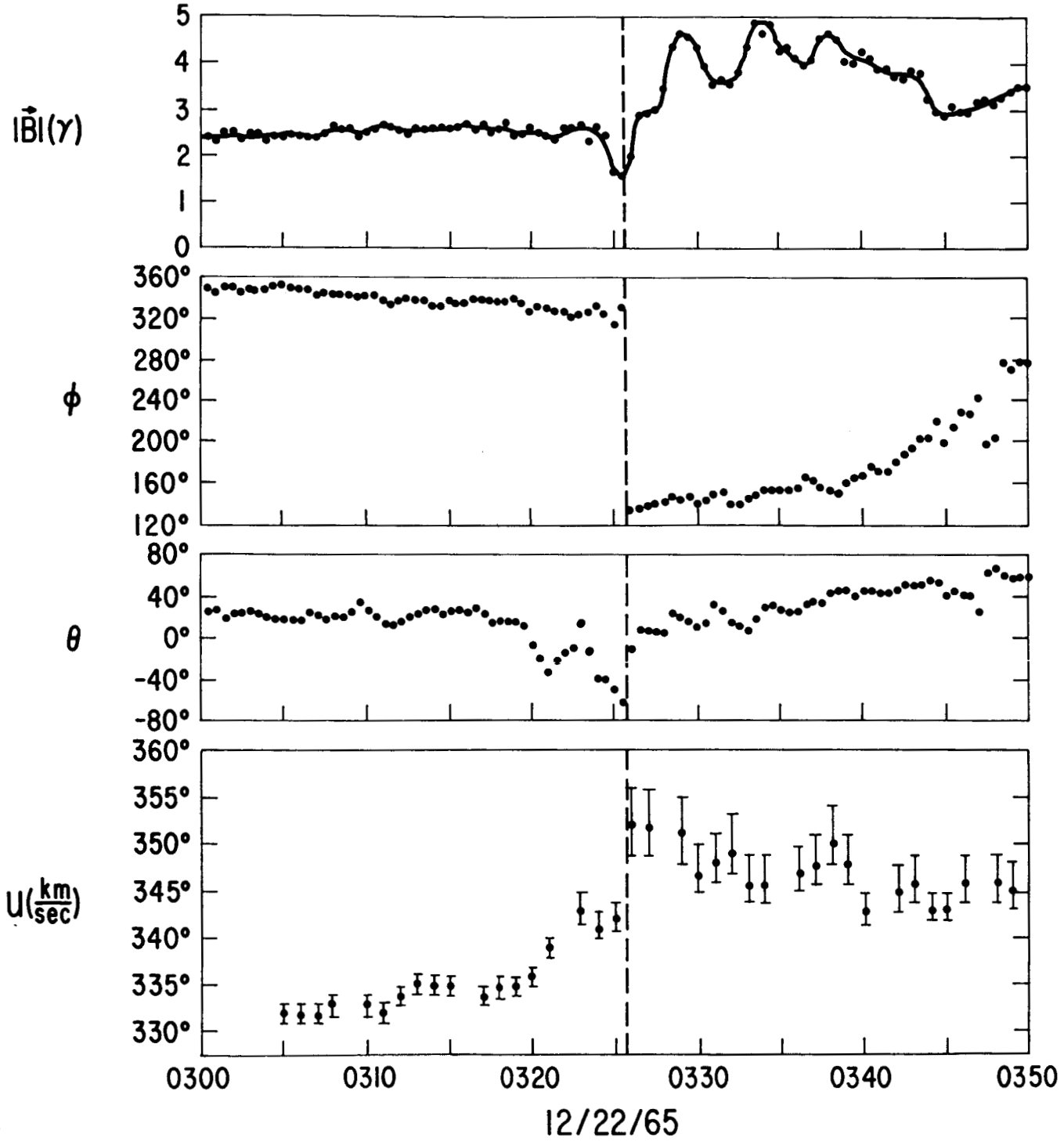
$|\vec{B}|(\gamma)$
5
4
3
2
1
0
ϕ
360°
320°
280°
240°
200°
160°
120°
θ
80°
40°
0°
-40°
-80°
U($\frac{km}{sec}$)
360°
355°
350°
345°
340°
335°
330°
0300
0310
0320
0330
0340
0350
12/22/65

FIGURE 19

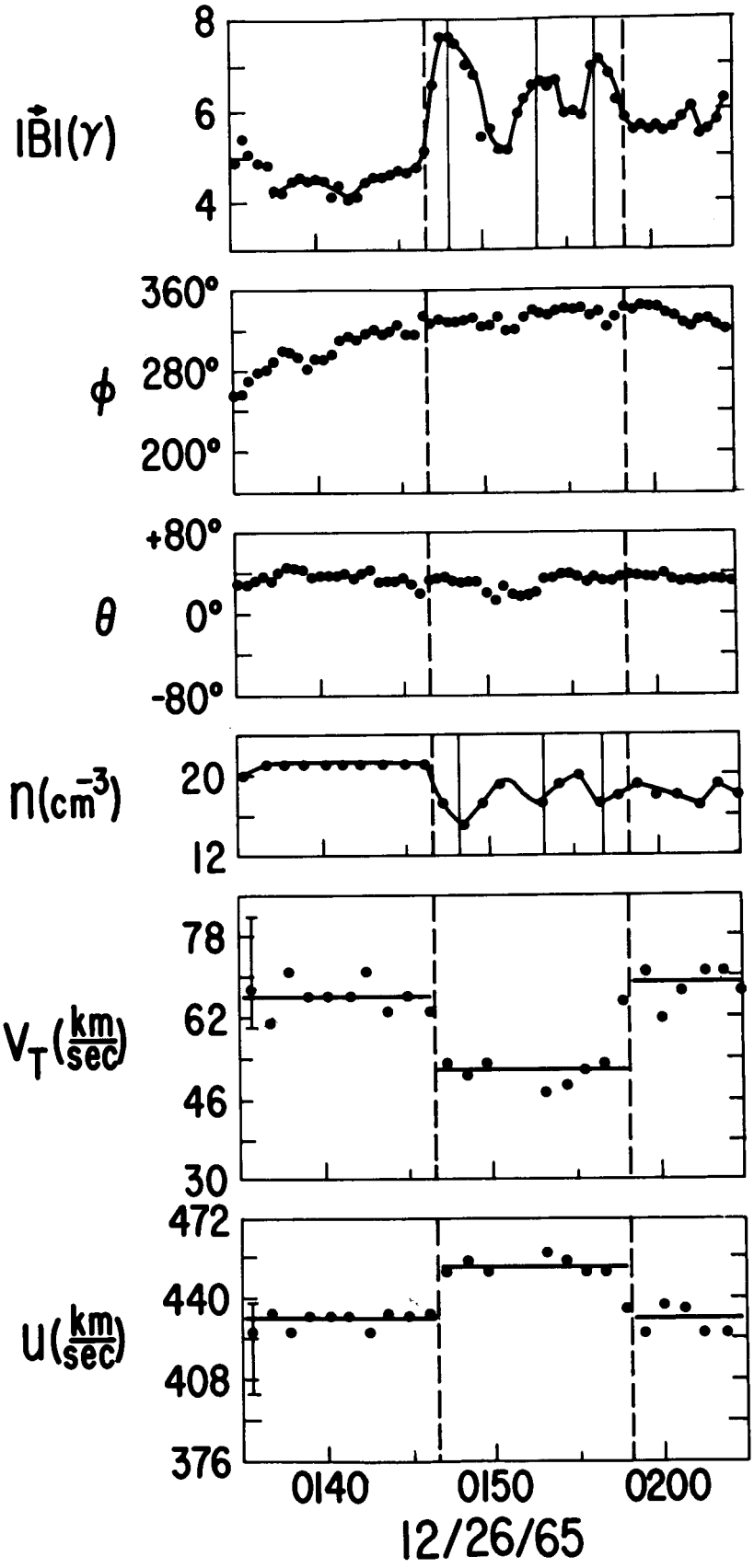
|B|(γ)
8
6
4
φ
360°
280°
200°
θ
+80°
0°
-80°
n(cm⁻³)
20
12
V_T (km/sec)
78
62
46
30
u (km/sec)
472
440
408
376
0140
0150
0200
12/26/65

FIGURE 20